The Calibration of the ARGUS Drift Chamber

H. Kapitza

April 22, 1994

Abstract

This report describes a revised procedure for the calibration of the ARGUS Drift Chamber. Several sources of drift time corrections have been identified. Taking all these into account when transforming measured time intervals to drift distances, eliminates many systematic effects which were observed with the old calibration scheme.

1 Introduction

This paper gives a detailed description of a revised calibration procedure for the ARGUS Main Drift Chamber (DC). The initially used calibration scheme has been briefly described in the ARGUS detector paper [1], and it was used for several years. During the development of the track and vertex fitting software for the newly added Micro Vertex Drift Chamber (μVDC) [2] and the Silicon Strip Vertex Detector (SSVD) it turned out that the DC track fit suffered from some serious systematic problems. These could be overcome by a critical evaluation and subsequent modification of the calibration procedure.

2 Basic Drift Chamber and Track Fit Features

Before describing the details of the new calibration scheme it is worthwhile to recall some basic features of the DC and of the track fit procedure. For more details refer to [1].

2.1 The ARGUS Drift Chamber

The ARGUS DC is a large volume cylindrical drift chamber ($r_{in} = 150\,\mathrm{mm}$, $r_{out} = 859\,\mathrm{mm}$, $z_{max} = 1000\,\mathrm{mm}$). It contains 5940 drift cells which are arranged in 36 concentric layers (see Table 1). Half of these are stereo layers which have the shape of hyperboloids with a geometrical sag

$$s = r_{max} - r_{min} = r(z = \pm z_{max}) - r(z = 0) = 4\,\mathrm{mm}. \tag{1}$$

With increasing radius this constant sag results in an increasing stereo angle

$$\alpha = \arctan\left(\frac{\sqrt{2sr_{min} + s^2}}{z_{max}}\right) = \arctan\left(\frac{\sqrt{2sr_{max} - s^2}}{z_{max}}\right). \tag{2}$$

The alternating axial and stereo layers are separated by layers of field wires which have the shape of hyperboloids with a geometrical sag of 2 mm. Figure 1 shows a schematic section

i	layer	r_{min} [mm]	r_{max} [mm]	$\Delta\phi$ [mrad]	ϕ_0 [mrad]	α [mrad]	HV [V]	# wires
36	19	808	812	23.271	0	80.325	2630	270
35	1	792	792	23.800	11.900	0	2680	264
34	20	772	776	24.353	0	−78.527	2700	258
33	2	756	756	24.933	0	0	2700	252
32	21	736	740	25.541	0	76.687	2700	246
31	3	720	720	26.180	0	0	2700	240
30	22	700	704	26.851	0	−74.800	2700	234
29	4	684	684	27.558	13.779	0	2700	228
28	23	664	668	28.303	0	72.864	2700	222
27	5	648	648	29.089	14.544	0	2700	216
26	24	628	632	29.920	0	−70.874	2700	210
25	6	612	612	30.800	0	0	2700	204
24	25	592	596	31.733	0	68.826	2700	198
23	7	576	576	32.725	0	0	2700	192
22	26	556	560	33.781	0	−66.714	2700	186
21	8	540	540	34.907	17.453	0	2700	180
20	27	520	524	36.110	0	64.532	2700	174
19	9	504	504	37.400	18.700	0	2700	168
18	28	484	488	38.785	0	−62.273	2700	162
17	10	468	468	40.277	0	0	2700	156
16	29	448	452	41.888	0	59.928	2700	150
15	11	432	432	43.633	0	0	2700	144
14	30	412	416	45.530	0	−57.487	2700	138
13	12	396	396	47.600	23.800	0	2700	132
12	31	376	380	49.867	0	54.936	2700	126
11	13	360	360	52.360	26.180	0	2700	120
10	32	340	344	55.116	0	−52.259	2700	114
9	14	324	324	58.178	0	0	2700	108
8	33	304	308	61.600	0	49.437	2700	102
7	15	288	288	65.450	0	0	2700	96
6	34	268	272	69.813	0	−46.442	2700	90
5	16	252	252	74.800	37.400	0	2700	84
4	35	232	236	80.554	0	43.240	2700	78
3	17	216	216	87.266	43.633	0	2700	72
2	36	196	200	95.200	0	−39.778	2680	66
1	18	180	180	104.720	0	0	2630	60

Table 1: Parameters of the ARGUS Drift Chamber layers

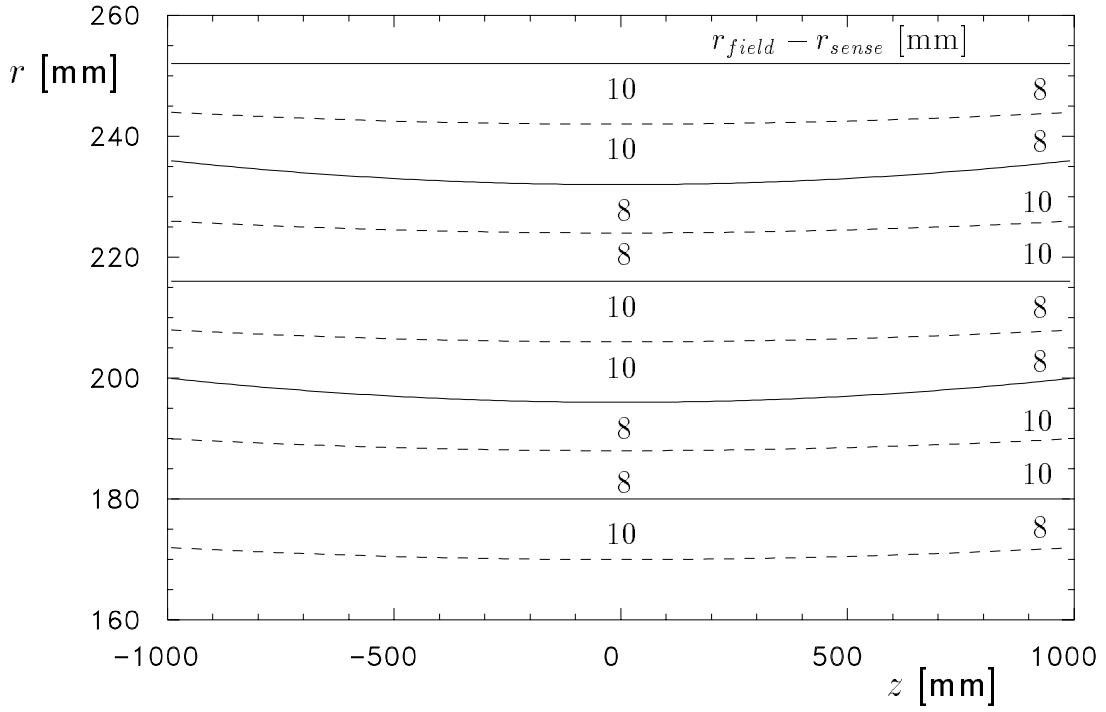

Figure 1: Schematic section through the innermost part of the ARGUS DC in the rz-projection. Solid lines are sense wire layers, dashed lines are field wire layers.

through the DC in the rz-plane, indicating how the radii of the innermost wire layers vary with z.

The radii and numbers of wires shown in Table 1 result in a very homogeneous design of the ARGUS DC. The whole chamber volume is occupied by almost identical drift cells. Their shape would be exactly the same everywhere if the chamber contained only axial layers with

$$N_i = 60 + (i-1) \cdot 6 \qquad (i = 1, \ldots, 36) \tag{3}$$

wires at the average radii

$$r_i = \frac{1}{2}[r_{min} + r_{max}] = [180 + (i-1) \cdot 18] \text{ mm} \, . \tag{4}$$

Then all cells would have a width of

$$w = \frac{2\pi r_i}{N_i} = \frac{2\pi \, [180 + (i-1) \cdot 18] \, \text{mm}}{60 + (i-1) \cdot 6} = 6\pi \, \text{mm} = 18.850 \, \text{mm} \tag{5}$$

and a height of

$$h = \Delta r = 18 \, \text{mm} \, . \tag{6}$$

In the real DC only the cell widths in the stereo layers,

$$w_i(z) = r_i(z) \cdot \Delta\phi_i \, , \tag{7}$$

deviate from these homogeneous conditions. Using the values for r_{min}, r_{max}, and $\Delta\phi$ as given by Table 1, one finds the strongest deviations in the innermost stereo layer: $w = 18.659 \ldots 19.040$ mm, but still the assumption of a uniform cell width (5) in the ARGUS DC is accurate within 1 %. The radial position of a sense wire within a drift cell exhibits much stronger local variations.

As can be seen from Figure 1, the radial displacement of axial wires from the cell centre varies between $\Delta r = -1\,\mathrm{mm}$ at $z = \pm z_{max}$ and $\Delta r = +1\,\mathrm{mm}$ at $z = 0$. The stereo wires behave just oppositely.

Figure 2 shows a drift cell of axial layer # 9 ($i = 19$) of the ARGUS DC in the plane $z = 0$. Here the sense wire is displaced by $\Delta r = +1\,\mathrm{mm}$ from the centre of the cell. Drift lines and isochrones for the nominal operating conditions are indicated as well. The almost quadratic cell cross section (aspect ratio $\pi/3$) leads to circular isochrones in a large fraction of the cell area.

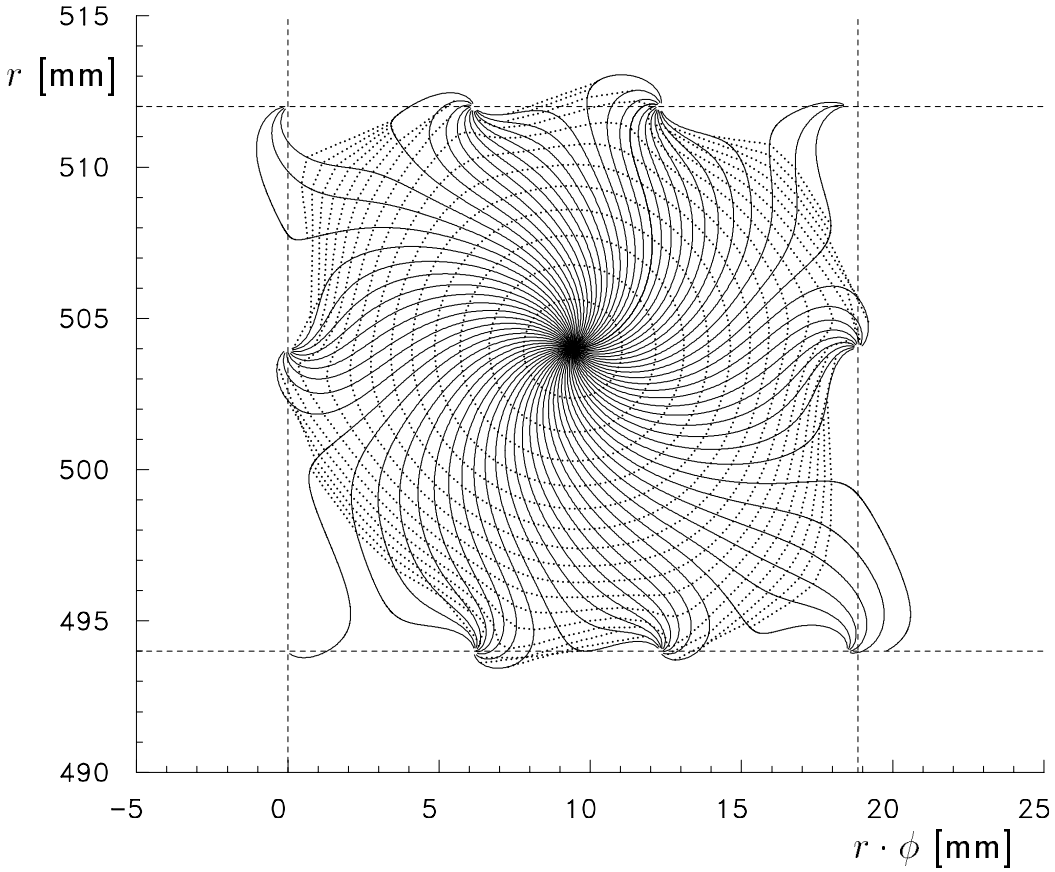

Figure 2: A typical drift cell of the ARGUS DC. Drift lines (in 5° steps) and isochrones (in 25 ns steps) were calculated for drift in pure propane with a magnetic field $B = 0.755\,\mathrm{T}$ and $\mathrm{HV} = 2700\,\mathrm{V}$. The dashed lines indicate the geometrical cell limits.

From the calibration point of view the homogeneity of the ARGUS DC allows one to handle all cells with the same basic calibration constants. Remaining local deviations are sufficiently well treated by additional small geometrical corrections.[1] Further constructional and operational details of the chamber will be discussed together with the implied calibration corrections.

2.2 The ARGUS Track Fit

Since the ARGUS Drift Chamber is placed in a 0.755 T magnetic field, charged particles move on helical trajectories. These are described by the following five parameters:

[1]The success of this approach is based on the alternating layer structure of the ARGUS DC which leads to about the same numbers of axial and stereo hits for all tracks. Then the basic calibration procedure always reliably averages over the different characteristics of both cell types. Chambers with different numbers of axial and stereo layers or with layers grouped into super-layers might be much less well-behaved.

δ : distance of closest approach to the first hit wire in the $r\phi$-projection;
ζ : z-coordinate of the helix point which in the $r\phi$-projection has the distance δ from the first hit wire;
κ : $= Q/p_t$, a measure for the helix curvature in the $r\phi$-projection ($Q = \pm 1$ is the particle charge and p_t its transverse momentum);
$\cot\theta$: θ is the polar angle with respect to the z-axis;
ϕ : azimuthal angle.

The parameters κ, $\cot\theta$ and ϕ are defined at the reference point specified by δ and ζ. For notational convenience the track parameters will be considered as components of a 5-dimensional vector $\vec{q}$.

Assume that pattern recognition has identified a set of N hit wires to originate from the passage of a charged particle. Then the track parameters are determined by an iterative least squares fit which minimizes the following χ^2-expression:

$$\chi^2 = \sum_{i=1}^{N} \frac{(d_{meas,i} - d_i(\vec{q}))^2}{\sigma_i^2} \; . \tag{8}$$

Here the $d_{meas,i}$ and σ_i denote the measured drift distances and their errors, respectively. The $d_i(\vec{q})$ are the calculated distances of closest approach to the hit wires, obtained from a tracing procedure which starts at the first hit wire and uses the parameter set $\vec{q}$ for track propagation. This procedure takes momentum loss and multiple scattering into account.

It is convenient to interpret the measured and calculated distances as components of N-dimensional vectors $\vec{d}_{meas}$ and $\vec{d}(\vec{q})$, respectively. The variances σ_i^2 of the measured distances are the diagonal elements of the $N \times N$ covariance matrix $\mathbf{V}(\vec{d}_{meas})$. Expression (8) can then be written as

$$\chi^2 = \left[\vec{d}_{meas} - \vec{d}(\vec{q})\right]^T \mathbf{V}^{-1}(\vec{d}_{meas}) \left[\vec{d}_{meas} - \vec{d}(\vec{q})\right] \tag{9}$$

where the superscript T denotes transposition.

Finally it should be mentioned that the iterative minimization of (8) or (9) implies a linearization of the generally non-linear track model $\vec{d}(\vec{q})$. Then the trajectories calculated from two track parameter sets $\vec{q}$ and $\vec{q}\,'$ are related by

$$\vec{d}(\vec{q}) = \vec{d}(\vec{q}\,') + \mathbf{A}(\vec{q} - \vec{q}\,') \tag{10}$$

where $\mathbf{A}$ is the matrix of derivatives with elements $A_{i\mu} = \partial d_i / \partial q_\mu$ ($i = 1, \ldots, N$ and $\mu = 1, \ldots, 5$). Close to the minimizing parameter set this is usually a very good approximation.

3 Track Reconstruction Problems

3.1 The Importance of Low Precision Tracking

Recent reconstruction software development at ARGUS aims at the precise determination of event vertices, using the data from two high precision devices, the μVDC and the SSVD. Track parameters with small systematic distortions and correctly calculated errors are an indispensable input for a reliable and precise vertex reconstruction procedure. This means on one hand that systematic effects in the μVDC and in the SSVD must be controlled to a quite high level of accuracy, but on the other hand one must keep in mind that in a complex tracking system

the high precision components also depend on the proper performance of low precision parts. In the ARGUS tracking system[2] there are several examples for this:

- Due to its long lever arm the DC is essentially the only device which contributes to the momentum measurement. μVDC and SSVD mainly improve the positional and directional track parameters.
- Pattern recognition in the μVDC uses reconstructed DC tracks and hence is strongly affected by systematic track parameter distortions.
- The result of the DC track reconstruction enters as an additional weight in the subsequent fit of the μVDC hits [1]. Wrongly determined DC track parameter errors result in a wrong weight.
- The alignment of the SSVD which itself produces only one measured point per track relies strongly on correct tracking in the DC and the μVDC.

These examples demonstrate how high precision devices cannot always compensate for systematics introduced by a lower precision detector. This motivated the investigation of systematic problems in the DC track reconstruction.

3.2 Track Fit Inconsistencies

A first problem readily showed up by inspecting the distributions of the normalized track parameter differences ("pulls") for collinear two-track events (Bhabhas, μ-pairs, cosmics). Denoting the parameter vectors of both tracks by $\vec{q}_1$ and $\vec{q}_2$ (both defined at the points of closest approach to the beam line), the pulls

$$\frac{q_{i,1} - q_{i,2}}{\sqrt{\sigma^2(q_{i,1}) + \sigma^2(q_{i,1})}} \stackrel{?}{=} N(0,1) \qquad (i = 1, \ldots, 5) \tag{11}$$

should be normally distributed with a mean value of zero and a standard deviation of one. The results obtained for μ-pairs are summarized in table 2. While the distributions are nicely cen-

i	parameter	mean value	standard deviation
1	δ	0.08	1.39
2	ζ	0.03	1.58
3	κ	0.29	1.47
4	$\cot\theta$	-0.02	1.63
5	ϕ	0.04	1.97

Table 2: Parameters of the pull distributions for μ-pairs (old calibration).

tered at zero[3], they are much broader[4] than to be expected from the individual track parameter errors.

[2] Typical intrinsic spatial resolutions of the SSVD, the μVDC and the DC are 20, 40 and 130 μm, respectively.

[3] The strongly different mean value for the κ pull distribution was caused by a rounding error problem which was hard to find but easy to eliminate.

[4] There is a non-statistical contribution to the very large widths of the $\cot\theta$ and ϕ pull distributions from remaining acollinear events in the used sample.

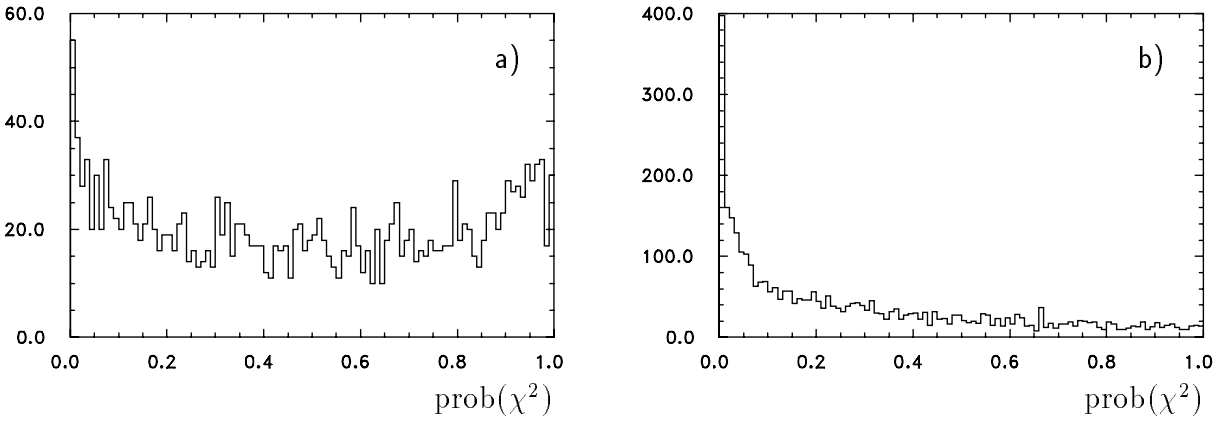

Figure 3: Fit probability distributions for (a) Barrel Bhabhas and (b) μ-pairs (old calibration).

This raised the question whether the DC measurement errors were determined correctly. Figure 3a shows the distribution of the probabilities calculated from the χ^2 values obtained by fitting tracks in a sample of Bhabha events registered in the barrel region of the detector. The flat distribution indicates that the fit weights are properly set, which is not surprising since these events served as a calibration sample. Figure 3b shows the same distribution for a sample of μ-pair events from the same run region using the same calibration constants. This distribution peaks towards zero, indicating a large fraction of bad fits. These could be caused by underestimated measurement errors or by ignored systematic effects. Initially it was hard to understand what kind of effects would make events with identical topology behave so differently.

3.3 Track Fit Anisotropy

However, there is one significant difference between Bhabha events on one side and μ-pairs (and other interesting event classes) on the other. Figure 4 shows the $\cos\theta$ distributions for the tracks in four different event samples. All distributions, except the one for the Bhabhas, are more or less flat. This means that from this point of view the calibration data sample is highly non-representative for potentially interesting analysis data samples.

This turns out to be a quite worrysome situation because Figure 5 demonstrates that the track fit quality depends strongly on the polar angle of the track. Here the mean fit probability is shown as a function of $\cos\theta$ for a sample of Barrel Bhabhas. For an isotropic behaviour of the DC one would expect these mean values to cluster around 0.5, thus reflecting a flat probability distribution in every $\cos\theta$ bin. This is obviously not the case.

Since such effects were not observed in (by definition perfectly calibrated) Monte Carlo data, it was concluded that they were not caused by the track fit procedure but by imperfections of the calibration. This led to a complete revision of the calibration procedure as will be described in the following.

4 General Remarks on Drift Chamber Calibration

Calibrating a drift chamber means to determine the following quantities:

- Several kinds of *time corrections* which for each hit convert the measured TDC count into a "drift time" t. A precise definition of t will be given in Section 6.2. The time t is the

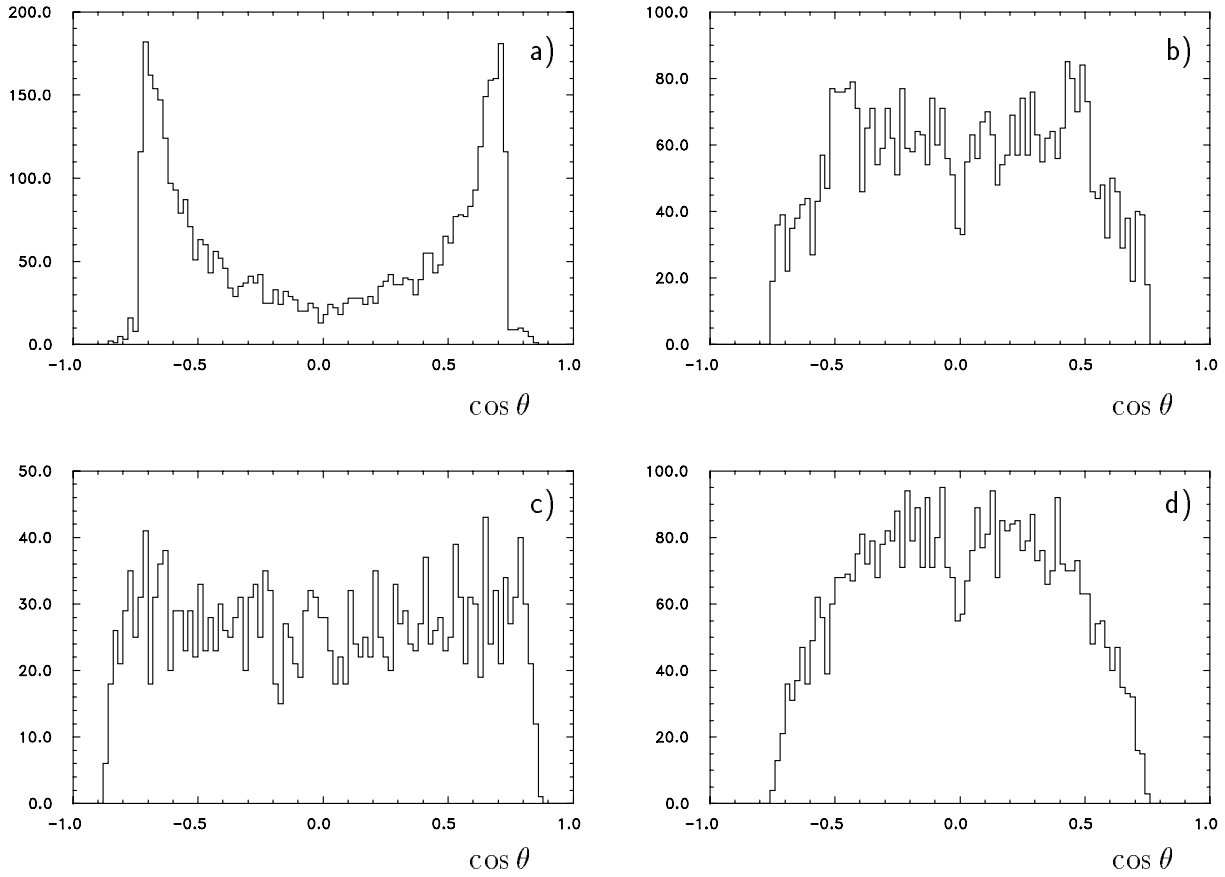

Figure 4: $\cos\theta$ distributions for (a) Barrel Bhabhas, (b) μ-pairs, (c) multi-hadron events and (d) cosmics.

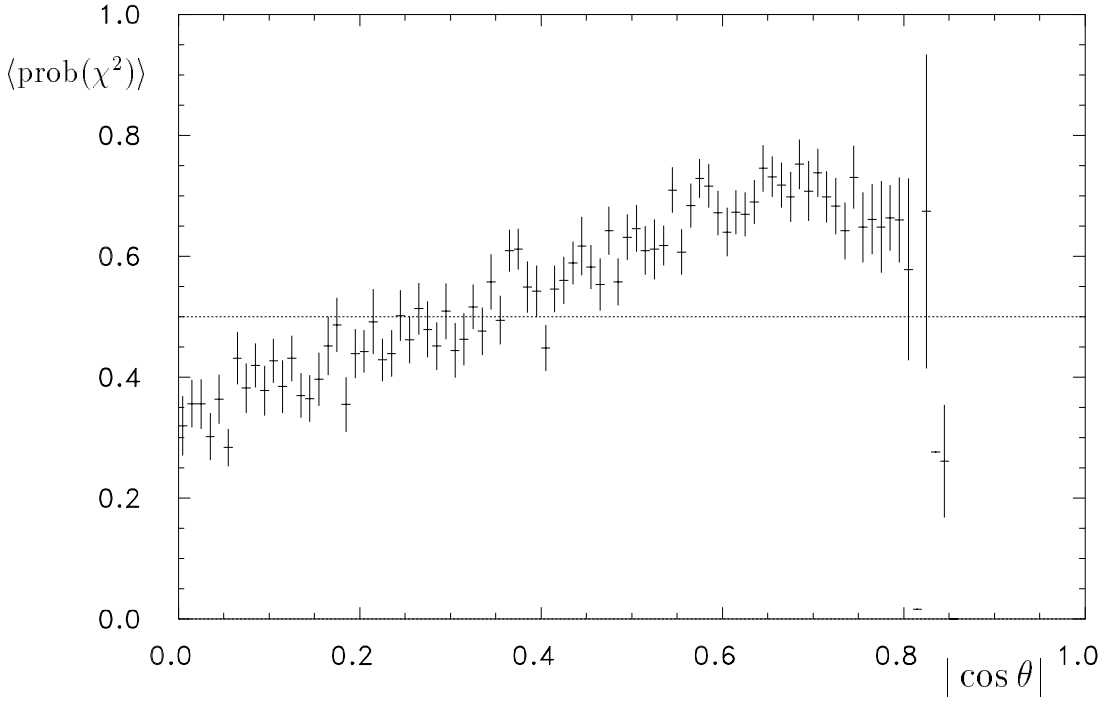

Figure 5: Mean fit probability vs. $|\cos\theta|$ for Barrel Bhabhas.

independent variable for the following sets of constants.

- The *distance-time-relation* (DTR) $d(t)$ which translates measured drift times t into drift distances d. In the ARGUS track reconstruction it is provided as a table with values for d given at 1 ns intervals. Since after the application of corrections the drift time t will in general be non-integral, interpolation is performed on the DTR table.

- The *resolution function* $\sigma(t)$ which provides the proper errors for the measured distances $d(t)$. In the ARGUS software the resolution function is also a table, with values of σ defined in 8 ns intervals.

- *Spatial corrections* which modify the drift distance d, obtained from the DTR, in order to compensate for effects which make the isochrones deviate from circles. This is particularly important in the outer drift cell regions where the electric field is no longer cylindrical.

- *Geometrical alignment constants* which describe the deviations of the actual chamber geometry (e.g. wire positions) from the nominal one.

For the ARGUS DC the DTR, the resolution function, the spatial and some of the time corrections are reasonably constant over quite long periods of time. Changes in these calibration constants can usually be related to changes in the DC operating conditions. On the other hand, some of the time corrections show more rapid fluctuations, mostly related to changes in the electronics[5]. The DC geometrical alignment constants are part of the detector description table.

It should be pointed out that due to the similarity of the drift cells throughout the ARGUS DC one can handle hits anywhere in the chamber volume using the same DTR and resolution function. Local deviations of the drift cell shapes are so small that they can be treated by the spatial corrections.

The following sections describe the determination of these calibration constants for the ARGUS DC.

5 Preparation of a Calibration Dataset

The old DC calibration procedure used Bhabha events from the barrel region of the detector for determining the DTR and the resolution function. Using such events has several advantages:

- Due to the large Bhabha cross section many events are accumulated in a relatively short time.

- Due to their unique signature Bhabha events can be easily selected from raw data tapes by a fast evaluation of the shower counter information. Together with the previous point this allows for a fast feedback between data taking and calibration.

- Due to the high momentum of the tracks one can neglect the systematic uncertainties introduced by multiple scattering and by non-radial traversal of drift cells.

While these are very attractive features for a calibration sample, there remains the problem that due to their strongly peaked polar angle distribution Barrel Bhabhas are not representative

[5]The ARGUS terminology is CDS for the long-term constants and CDT for the short-term constants.

for most event classes of interest. Since in Section 3.3 it was shown that there clearly are polar angle dependent effects in the track reconstruction, one should rather use an event sample with a flat polar angle distribution for the calibration, instead of relying on a proper determination of the polar angle dependent corrections at a later stage.

A calibration data sample with a flat $\cos\theta$ distribution is easily created by applying polar angle dependent rejection weights while selecting Barrel Bhabha events. On raw data level one obtains the polar angle information from the positions of the hit shower counter modules. Experience has shown that 2500 events are sufficient for the determination of one set of calibration constants.

6 Calibration Independent Time Corrections

The measured TDC values must be corrected for several effects in order to obtain the drift time t which is the proper independent variable for the DTR and the resolution function. In this section those time corrections will be discussed which are independent of the operating conditions of the DC itself.

6.1 Event Trigger Time

The TDCs of the ARGUS DC (LeCroy System 4290 with 1024 ns full scale, 1 ns/count) operate in Common Stop mode, i.e. the wire signals are used to start individual TDCs while a delayed coincidence of trigger and bunch crossing signals stops all TDCs. Although the coincidence is adjusted such that the very precisely timed bunch crossing signal determines the stop time, there remains a stop time jitter of about 1 ns, caused by trigger source dependent transit times in the coincidence unit[6].

For each event the stop time is measured with respect to the bunch crossing.[7] Figure 6 demonstrates that the stop time jitter is very small for a particular trigger combination, while different triggers lead to clearly distinct stop times. Since one is only interested in relative times, a long-term average (determined from Barrel Bhabhas) is subtracted from the measured trigger times before they are added to all measured TDC values[8]. This procedure removes the trigger type dependence of the measured drift times on an event-by-event basis.

The situation is slightly different for cosmic events which are accepted by the normal data taking triggers. These are very useful monitoring events because they are strictly collinear and cover a wide momentum region, so they are worth being analyzed as well. Since cosmic events are not correlated with the bunch crossing, the coincidence of this signal with the trigger generally yields a wrongly timed stop signal for the TDCs. The best measure of the event time relative to the bunch crossing is given by the average time measured in the ARGUS time-of-

[6] This unit also performs a logical OR of the four ARGUS trigger sources: ETOT, CPPT, HESH, and CMAT. See ref. [1] for more details.

[7] A time dependent malfunction of the central trigger-OR spoiled the measurement of these times for some trigger classes in certain parts of experiments 9 – 11. Here the times for the affected triggers were determined from a similar procedure as described for the layer time shifts in Section 7.8. They are hard-coded in the unpack routine `DTUNPK`.

[8] In the ARGUS software the measured trigger time is held in the variable `BUNCH1`, the long-term average in `TIDBUN` and the relative trigger time in `TIDTCO`. Bad measurements (relative trigger times outside ± 3 ns) are ignored.

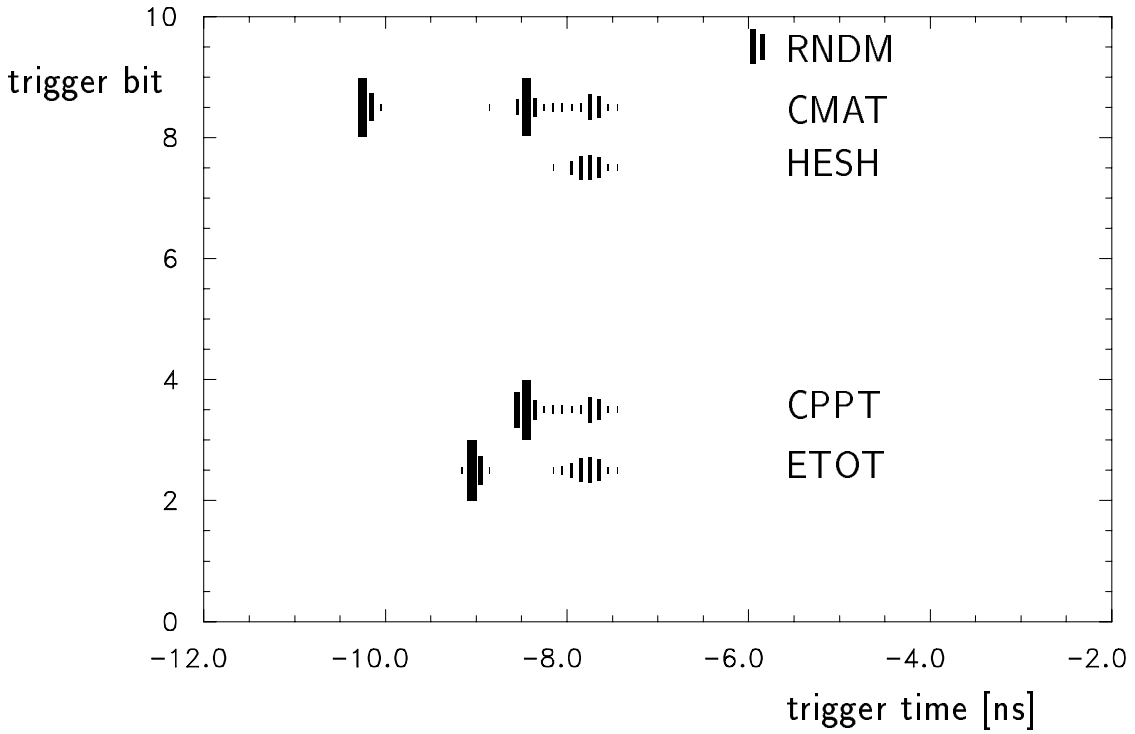

Figure 6: Trigger bits vs. trigger time (before subtraction of long-term average).

flight (TOF) system[9]. Adding this time to all measured TDC values eliminates the event time dependence of the measured drift times. This procedure implies that cosmic tracks cannot be properly analyzed before the TOF analysis has been performed, i.e. one cannot use raw data tapes.

6.2 Crate Time Shift

The ARGUS DC TDCs occupy nine crates, each with its own controller. Within one crate the characteristics of all signal channels are well equalized by regular application of a trimming procedure (using the Autotrim feature of the TDCs together with test pulses fed to the preamplifier inputs). Due to slightly different signal delays in the controllers and in the channels of the fan-out circuitry which distributes the stop signal to the nine crates, one needs nine constants for equalizing crate dependent differences in the measured times. They are obtained by fitting a function

$$f(TDC) = \left[\frac{a_1}{(TDC - a_2)^2} + a_3\right] \cdot 0.5\,\mathrm{erfc}\left(\frac{TDC - a_4}{a_5}\right) \tag{12}$$

to the trigger time corrected raw TDC spectrum of each crate. Figure 7 shows an example of such a fit. For all crates the constants $950 - a_4$ are stored[10]. Adding these to the measured TDC values effectively shifts all spectra upon each other, with the right edge reaching half the maximum at a TDC count of 950.

[9] In the ARGUS software this time is the mean value of the `NDTTOF` times stored in `DTTOF(100)` in `COMMON/CDTTOF/`.

[10] In the ARGUS software they are kept in the array `NTIDCR(9)`.

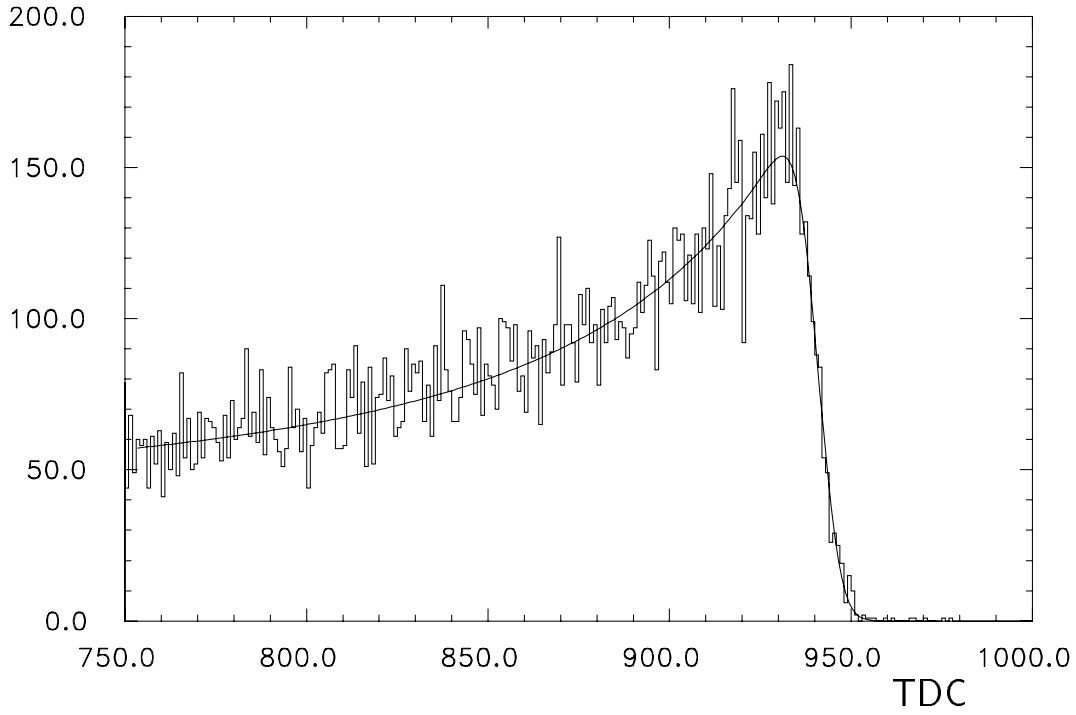

Figure 7: Trigger time corrected raw TDC spectrum for crate 3 with fit.

It should be noted that in Common Stop mode large TDC values correspond to small drift times and distances. However, for the evaluation of the DC TDC information it is not necessary to invert the time scale. Hence throughout this report the term "drift time" always refers to the time

$$t = T_0 - t_{drift} \tag{13}$$

where t_{drift} is the physical drift time and $T_0 \approx 950\,\mathrm{ns}$.

6.3 Signal Propagation Time

The preamplifiers of the ARGUS DC are mounted on the chamber end plates. The axial wires are read out on the $+z$ side, the stereo wires on the $-z$ side. Depending on the z-coordinate of a hit this leads to a different effect of signal propagation times in the sense wires for axial and stereo wires. The measured drift times are normalized to the case of hits occurring at $z = 0$ if for axial (stereo) wires the signal propagation time

$$t_{prop} = \frac{z}{v_{prop}} \tag{14}$$

is added to (subtracted from) the measured TDC values. Best results are obtained for $v_{prop} = 24\,\mathrm{cm/ns} = 0.8 \cdot c$.[11] This correction can only be applied after pattern recognition has been performed, since one needs at least a rough estimate of the z-coordinate of the hit.

[11] For the old ARGUS VDC a value $v_{prop} \approx 0.7 \cdot c$ was measured from the time difference of direct signals and those reflected at the open sense wire end.

6.4 TOF Correction

If a particle with velocity $v = \beta c$ has travelled a spatial path length s from the interaction region to the point of closest approach to a sense wire, the signal from that wire (TDC Start) will be delayed by the flight time

$$t_{flight} = \frac{s}{\beta c} \ , \tag{15}$$

compared to the case of instantaneous passage of the particle. In order to normalize all measured times to the latter case, one must add the time of flight to the measured TDC values. In the initial phase of the track fit $\beta = 1$ is assumed, but the correction is re-evaluated at a later stage when a better value for β is available from the dE/dx analysis.

In the analysis of cosmic tracks one must be aware that one of the tracks (usually the upper one) has a "reversed" timing, i.e. the outer DC layers are traversed first. In that case one must subtract the flight times (15) from the measured TDC values.

7 Distance Time Relation and Resolution Function

7.1 Residuals

The determination of the DTR and of the resolution function — the basic calibration constants — is based on the concept of *residuals*. Before defining these, a few words must be said about the sign convention for drift distances. Each drift time measurement yields only an unsigned quantity, namely the radius $d(t)$ of a circle around the sense wire which the particle trajectory must be tangent to. Such a measurement does not tell us on which side the particle passed the wire. This *left-right ambiguity* does not exist for the fitted track which is calculated from a given track parameter set $\vec{q}$. Here one does not only know the unsigned distances of the track from the hit wires but really the spatial points of closest approach. Hence it is meaningful to introduce a drift distance sign which indicates the side of a wire on which a track passed. The ARGUS DC track fit sign convention is illustrated by Figure 8. If one looks against the wire

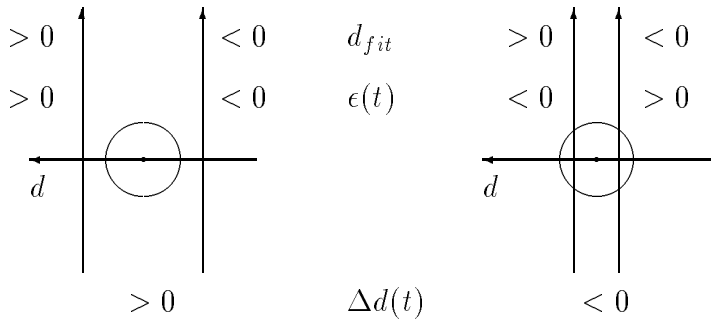

Figure 8: Drift distance and residual signs in the ARGUS DC track fit for four different cases.

and follows the track along its momentum vector, the distance from the wire is positive if the track passes on the left side and negative if it passes on the right side of the wire. For each track-wire combination, described by the local track direction $\vec{t}$ and the wire direction $\vec{w}$, this prescription introduces a local d-coordinate axis having its origin at the wire and pointing in

the direction $\vec{w} \times \vec{t}$. The measured drift distance $d(t)$ always gets the same sign assigned as the fitted distance $d_{fit} = d(\vec{q})$.

The *residual* $\epsilon(t)$ is defined to be the difference of fitted and signed measured drift distance:

$$\epsilon(t) \equiv d_{fit} - d_{meas} = d_{fit} - \text{sign}\,(d_{fit}) \cdot d(t) = \text{sign}\,(d_{fit}) \cdot (|d_{fit}| - d(t)) \ . \tag{16}$$

For each hit $\epsilon(t)$ represents the deviation of fit and measurement along the local d-coordinate axis which enters the χ^2-expression (8). On the other hand, the *distance correction*

$$\Delta d(t) \equiv \text{sign}\,(d_{fit}) \cdot \epsilon(t) = |d_{fit}| - d(t) \tag{17}$$

indicates whether the radius of a drift circle is too small or too large. This is the relevant quantity for additively correcting an approximate DTR.

For the determination of the DTR and the resolution function it is important to understand some features of the $\Delta d(t)$ distributions. In the central drift cell region their shape is approximately Gaussian, as shown by Figure 9a. Going closer to the sense wire, the curvature

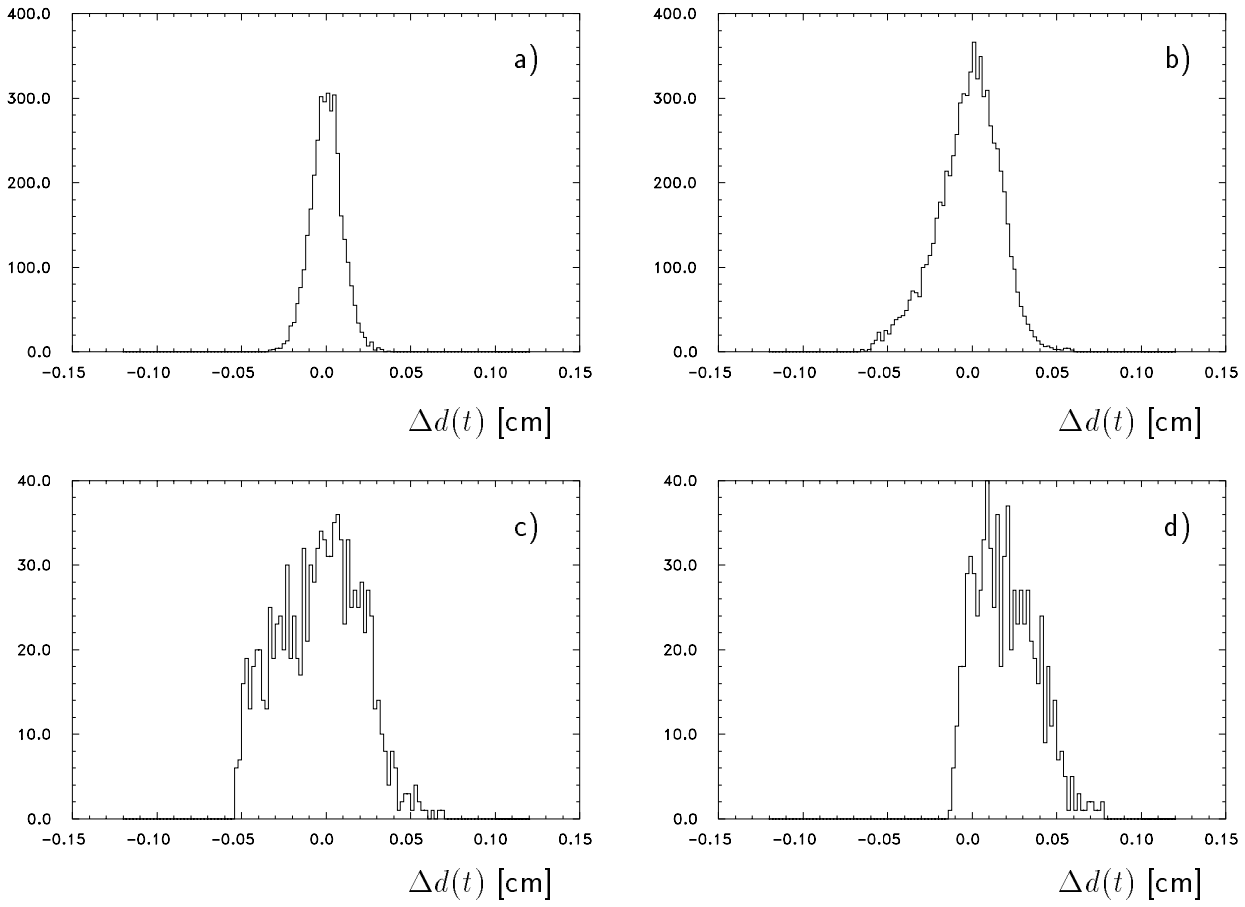

Figure 9: $\Delta d(t)$ distributions for (a) $800 \leq t < 808\,\text{ns}$ ($\equiv 0.5795 \leq d < 0.6007\,\text{cm}$), (b) $928 \leq t < 936\,\text{ns}$ ($\equiv 0.1121 \leq d < 0.1554\,\text{cm}$), (c) $946 \leq t < 947\,\text{ns}$ ($\equiv 0.0438 \leq d < 0.0510\,\text{cm}$) and (d) $951 \leq t < 952\,\text{ns}$ ($\equiv d < 0.0078\,\text{cm}$). Drift distances are taken from the final DTR.

of the isochrones increases, and a significant contribution to the signal arises from ionizations occurring at distances larger than d_{fit}, the distance of closest approach to the wire. Then the measured distance tends to be systematically larger than the fitted one, and the $\Delta d(t)$ distribution becomes asymmetric with a tail on the negative side (see Figure 9b). Finally, for very

small drift distances, the negative tails of the distributions are "folded over" to the positive side since according to (17) $\Delta d(t)$ cannot be smaller than $-d(t)$.[12] This is demonstrated by Figures 9c and 9d.

Since positive and negative fitted distances are equally probable, it follows from (16) that the distributions of residuals $\epsilon(t)$ are always symmetric with respect to zero. Their shapes are those of superpositions of the corresponding distributions for $\Delta d(t)$ and $-\Delta d(t)$.

7.2 The Iterative Calibration Procedure

The DTR and the resolution function are determined in an iterative procedure. In each iteration the events of the calibration data sample are processed using an approximate DTR and resolution function. During event processing the following quantities are accumulated:

- The average distance corrections $\langle \Delta d(t) \rangle$ in 1 ns bins of the drift time t.
- The average drift time $\langle t \rangle$ in 200 μm bins of the fitted drift distance $|d_{fit}|$.
- Distributions of scaled residuals in 8 ns bins of the drift time t. The scaling factor will be discussed in Section 7.6. For times $t \geq 936$ ns, corresponding to drift distances $d \leq 0.1121$ cm, these distributions are also accumulated in 1 ns bins of the drift time.

After processing all data the accumulated quantities are evaluated. This yields corrections to be applied to the input calibration constants. These corrected (better) constants are used as input for the next iteration. The procedure stops if the calibration constants do no longer change from one iteration to the next.

7.3 Track Quality Cuts

Since the calibration data sample is selected from raw data without using any track information, one must apply some cuts in order to reject bad tracks from the calibration procedure:

- The tracks should originate in the nominal interaction volume ($\delta \leq 1.5$ cm, $\zeta \leq 5.0$ cm, both parameters defined with respect to the origin). The innermost hit should be at a radius $15 < r < 25$ cm. These cuts make sure that the TOF correction is meaningful.
- Each track must have at least 12 axial and 12 stereo wires hit. In some special applications this cut is relaxed, and a restriction of the polar angle region to $|\cos\theta| < 0.92$ becomes effective (see Section 9.3).
- Except for the determination of the geometrical corrections, the transverse momentum must exceed 2 GeV/c and there must be no multiple scattering kinks. This avoids uncertainties from non-radial penetration of the drift cells.

7.4 Integrated Time Spectrum

If an approximate DTR is not yet available, it can be obtained by integrating the measured time spectrum dN/dt. Writing the time spectrum as

$$\frac{dN}{dt} = \frac{dN}{dd(t)} \cdot \frac{dd(t)}{dt} \tag{18}$$

[12] This is a consequence of always giving d_{meas} the sign of d_{fit}.

and assuming a spatially homogeneously irradiated drift cell ($dN/dd = const$), one finds that the time spectrum is proportional to the drift velocity dd/dt. Integration and proper normalization yields

$$d(t) = \frac{d_{max}}{N_0} \int_t^{t_{max}} \frac{dN}{dt'} dt', \tag{19}$$

where t_{max} is the largest considered measured time, d_{max} the largest drift distance, and N_0 the number of spectrum entries between 0 and t_{max}. The $d(t)$ values are calculated in 1 ns intervals of t and then smoothed using cubic splines. This yields a reasonable approximate DTR. The resolution is assumed to be constant ($\sigma = 250\,\mu$m) in this "cold start" situation.

7.5 Distance Time Relation

A correctly determined DTR must properly parametrize the observed correlation between measured drift times and fitted distances as shown by Figure 10. In particular the continuous behaviour around $d_{fit} = 0$ should be reproduced. In this region some complications arise from the fact that the DTR, the unsigned function $d(t)$, must describe a correlation involving the quantity d_{fit} which acquires a sign through the track fit.

Using the accumulated average distance corrections for updating the input DTR according to

$$d(t)_{out} = d(t)_{in} + \langle \Delta d(t) \rangle \tag{20}$$

only works properly as long as the $\Delta d(t)$ distributions are symmetric with respect to the position of their maximum. Only then a correct DTR, characterized by $\langle \Delta d(t) \rangle = 0$, will remain unchanged from one iteration to the next. As a consequence, updating the DTR according to (20) fails for small drift distances because there the $\Delta d(t)$ distributions are definitely asymmetric (see Figures 9b–d).

It is instructive to formulate the problem in a slightly different way. By insertion of the definition (17) one finds that the updating prescription (20) is equivalent to

$$d(t)_{out} = \langle |d_{fit}| \rangle \ , \tag{21}$$

i.e. at each time t the input DTR value is just replaced by the average unsigned fitted distance. However, due to the truncation at $|d_{fit}| = 0$ the average values $\langle |d_{fit}| \rangle$ are always larger than zero, and updating the DTR according to (21) leads to an artificial increase of small drift distances, as shown by the crosses in Figure 11. This clearly does not describe the continuous transition between positive and negative distances as observed in the measured time-distance correlation, but tends to separate both branches at $d_{fit} = 0$.

The smooth distribution of entries around $d_{fit} = 0$ in Figure 10 is much better described by the average drift time $\langle t \rangle$ in bins of $|d_{fit}|$. Inversion of this function $t(d)$ yields the best parametrization of the DTR at small distances. Further away from the wire the results from the inversion of $t(d)$ agree with those of the updating method discussed above, as shown by Figure 11.[13] The problematic region for the function $t(d)$ is at large distances where the branches of the measured time-distance correlation run almost parallel to the t-axis.

For the ARGUS DC the updating of the input DTR proceeds as follows: The function $t(d)$ is obtained from a cubic spline fit (with 20 equidistant knots) to the average drift times $\langle t \rangle$ in

[13] In this figure one recognizes some features of the $\Delta d(t)$ distributions which were discussed in connection with Figure 9: As the negative tails develop, the values $d(t)_{in} + \langle \Delta d(t) \rangle = \langle |d_{fit}| \rangle$ drop below the inverted $t(d)$ function, until at $t = 947$ ns truncation of the tails reverses the situation.

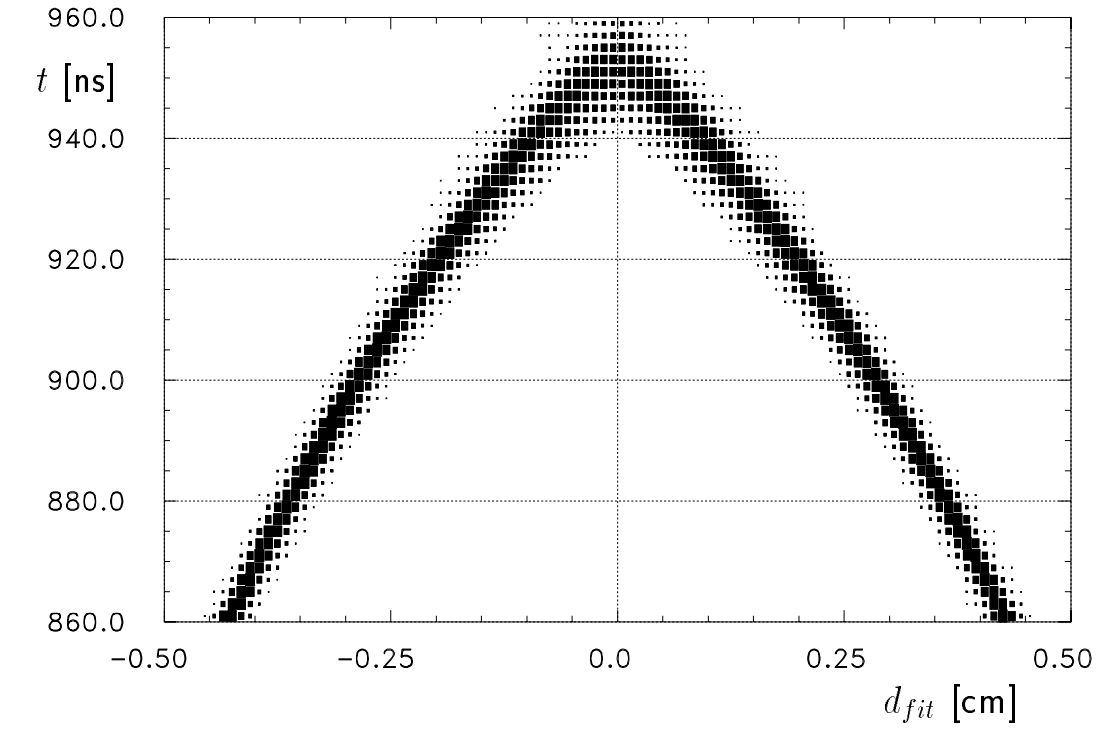

Figure 10: Observed correlation of measured drift times and fitted distances.

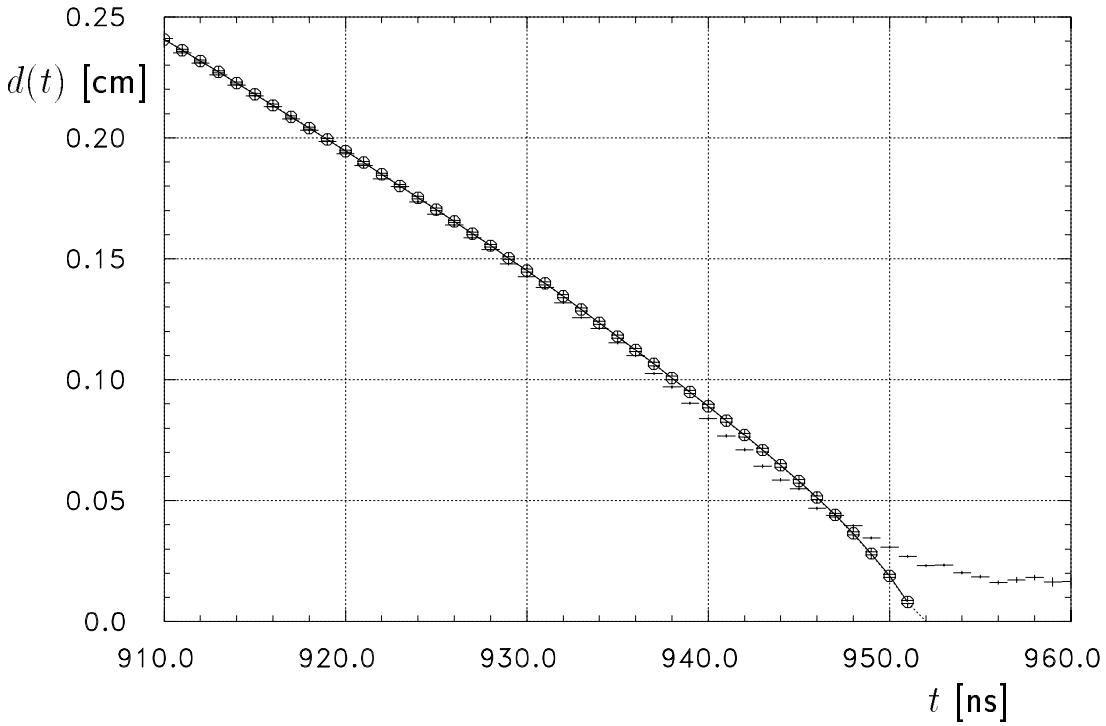

Figure 11: DTR close to the wire: $d(t)_{in} + \langle \Delta d(t) \rangle = \langle |d_{fit}| \rangle$ (crosses), inverted $t(d)$ function (circles), result of spline fit (solid line).

bins of $|d_{fit}|$. Then $t(d)$ is inverted numerically in order to yield the $d(t)$ values for distances $d < 0.3\,\mathrm{cm}$. The remaining $d(t)$ values are obtained by updating according to (20). Then all $d(t)$ values are smoothed by a cubic spline fit (with 40 knots placed at times corresponding to a uniform spacing in d). From the smoothing result the values $d(t)_{out}$ are calculated in 1 ns intervals and stored as new DTR.[14]

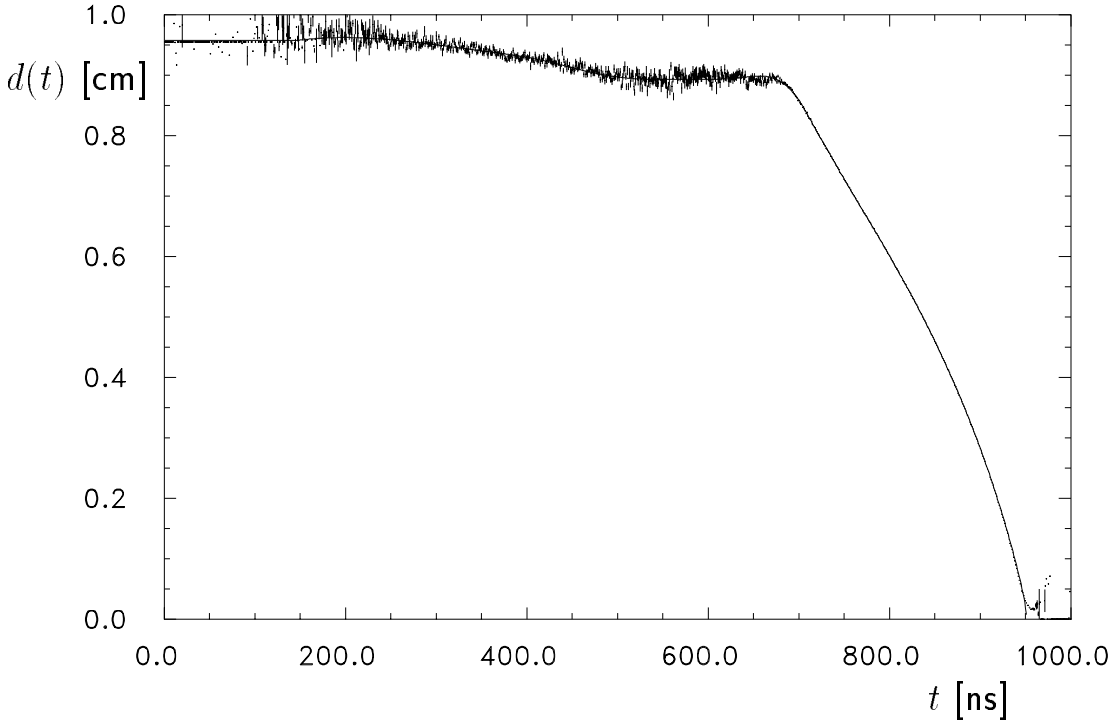

Figure 12: DTR after 5 iterations of the calibration procedure (solid line) and measured $|d_{fit}|$ values (error bars).

Figure 12 shows the DTR obtained after five iterations of the calibration procedure, starting with the integrated time spectrum. For better starting values convergence is reached after one or two iterations. The fast convergence of the procedure is largely due to the wire staggering properties of the DC (see Table 1). For most tracks the numbers of wires with positive and negative drift distances are about equal, and even a very crude approximation of the DTR is pulled very quickly towards the truth.

In Figure 12 one readily identifies four regions of distinctly different behaviour of the DTR:

- For times $680 < t < 950\,\mathrm{ns}$ (corresponding to distances $0 < d < 0.89\,\mathrm{cm}$) the DTR is nicely monotonous with an average drift velocity of $33\,\mu\mathrm{m/ns}$.
- Drift times $520 < t < 680\,\mathrm{ns}$ on average yield almost the same drift distance $d = 0.89\,\mathrm{cm}$. In this cell region the magnetic field squeezes the isochrones closely together (see Figure 2). As will be seen, this is a region of extremely bad spatial resolution.
- For times $200 < t < 520\,\mathrm{ns}$ (corresponding to distances $0.89 < d < 0.95\,\mathrm{cm}$) the DTR again behaves monotonously, although with a much smaller average drift velocity. These late signals are mainly due to charges created in the upper left and lower right corners of

[14] In the ARGUS software the DTR values are kept in `TIDRI(1024)`.

the drift cell shown in Figure 2. Here the electric field is very low and the drift velocity correspondingly small.

- For drift times below 200 ns the DTR is assumed to be constant since due to the lack of enough data it cannot be reliably updated.

7.6 Residual Scaling Factor

For each track to be fitted the resolution function $\sigma(t)$ serves to construct the (diagonal) covariance matrix $\mathbf{V}(\vec{d}_{meas})$ which appears in the χ^2-expression (9). The matrix elements $V_{ii}(\vec{d}_{meas}) = \sigma^2\left[d_i(t)\right]$ are the expectation values of the squared deviations of measured and true distances of closest approach to the hit wires. Since the true particle trajectory, described by the parameter set $\vec{q}_T$, by definition has no error, one can write

$$\mathbf{V}(\vec{d}_{meas}) = \mathbf{V}(\vec{d}_{meas} - \vec{d}(\vec{q}_T)) = \mathbf{V}(\vec{\epsilon}_T)\ , \tag{22}$$

i.e. at each drift time t the resolution function value $\sigma(t)$ equals the standard deviation of the distribution of the *true* residuals $\epsilon_T(t)$.

For the iterative determination of the resolution function this observation is of no direct use since the true residuals cannot be measured. In order to obtain a measurable quantity the unknown true track is replaced by the fitted track, described by the parameter set $\vec{q}$ which results from the last track fit iteration. These *measured* residuals (see also definition (16)) are related to the covariance matrix

$$\mathbf{V}(\vec{\epsilon}) = \mathbf{V}(\vec{d}_{meas} - \vec{d}(\vec{q})) \neq \mathbf{V}(\vec{d}_{meas})\ . \tag{23}$$

However, by means of the linearization (10) one can express the true residuals by measurable quantities:

$$\vec{\epsilon}_T = \vec{d}_{meas} - \vec{d}(\vec{q}_T) = \vec{d}_{meas} - \left[\vec{d}(\vec{q}) + \mathbf{A}(\vec{q}_T - \vec{q})\right] = \vec{\epsilon} - \mathbf{A}(\vec{q}_T - \vec{q})\ . \tag{24}$$

Error propagation in its most general form [3] then yields

$$\mathbf{V}(\vec{\epsilon}_T) = \mathbf{V}(\vec{\epsilon}) + \mathbf{V}(\mathbf{A}\vec{q}) = \mathbf{V}(\vec{\epsilon}) + \mathbf{A}\mathbf{V}(\vec{q})\mathbf{A}^T\ . \tag{25}$$

This equation describes the fact that our reference trajectory $\vec{d}(\vec{q})$ is only known within the transformed track parameter errors. Leaving this uncertainty aside, i.e. taking just the standard deviations of the measured residual distributions for updating the resolution function values, clearly underestimates the resolution. More details about this subject can be found in [4].

It is convenient to express the relation between measured and true residuals by multiplicative scaling factors. The requirement

$$V_{ii}(\vec{\epsilon}_T) \stackrel{!}{=} f_i^2 \cdot V_{ii}(\vec{\epsilon}) = f_i^2\left[V_{ii}(\vec{\epsilon}_T) - (\mathbf{A}\mathbf{V}(\vec{q})\mathbf{A}^T)_{ii}\right] \tag{26}$$

results in a factor

$$f_i = \sqrt{\frac{\sigma_i^2}{\sigma_i^2 - (\mathbf{A}\mathbf{V}(\vec{q})\mathbf{A}^T)_{ii}}} \tag{27}$$

to be applied to the i-th measured residual ϵ_i of a track before filling it into the appropriate distribution.

If the full covariance matrix of the track parameters is not available[15] one can nevertheless determine a global residual correction factor which is then valid for all hits of a track. Assuming that all N hits have the same Gaussian distributed error σ and that the average squared measured residual is ϵ^2, the condition

$$\chi^2_{min} = N \frac{\epsilon^2}{\sigma^2} = n_{dof} = N - 5 \tag{28}$$

(n_{dof} is the number of degrees of freedom of the fit) yields the correction factor

$$f_{track} = \frac{\sigma}{\epsilon} = \sqrt{\frac{N}{n_{dof}}} \; . \tag{29}$$

The average values from a large number of tracks are in good agreement for both methods, although correcting each hit individually is clearly the better procedure.

7.7 Resolution Function

In each iteration of the calibration procedure the new resolution function $\sigma(t)_{out}$ is determined from the widths of the measured distributions of scaled residuals $f \cdot \epsilon(t)$ which are accumulated in 8 ns bins of the drift time t. The simplest and at the same time most general method is to update the resolution function with the RMS errors of the residual distributions, since these estimators of the standard deviations do not depend on the actual distribution shapes. This is particularly relevant in the cell region close to the sense wire where the distributions have a complicated non-Gaussian shape (see Figure 9). In the central cell region where the residual distributions are approximately Gaussian, the RMS errors were checked against the widths obtained from Gaussian fits, and perfect agreement was found. This is an important check because the ARGUS track fit procedure rejects all hits with residuals $\epsilon(t) > 3\sigma(t)$, i.e. the measured residual distributions are actually truncated. Hence the usage of the RMS errors has the potential to underestimate the resolution, a situation which must be strictly avoided.

The obtained values for $\sigma(t)$ are smoothed using a cubic spline fit.[16] From the smoothing result the values $\sigma(t)_{out}$ are calculated in 8 ns intervals and stored as new resolution function.[17]

Figure 13 shows the extracted $\sigma(t)$ values and the result of the spline fit for the resolution function corresponding to the DTR of Figure 12. The already discussed drift time regions of distinctly different DTR behaviour also show up for the resolution function. The resolution is particularly bad in the time range $500 < t < 680$ ns where the DTR almost constantly yields a drift distance $d = 0.89$ cm. For times $t < 280$ ns no meaningful $\sigma(t)$ values can be determined due to lack of statistics.

Figure 14 shows how the already discussed behaviour of the ionization and the drift distance sign selection procedure (see Section 7.1) affect the resolution function close to wire. In order to reveal this in sufficient detail, the residual distributions for drift times $t \geq 936$ ns are also recorded in 1 ns bins. Approaching the sense wire one observes the following behaviour of the resolution function:

[15] In the ARGUS track fit this is the case if the fitted track has kink angles from multiple scattering.

[16] This spline fit uses the NAGLIB routine `E02BEE` which chooses the number and positions of knots according to a smoothness factor (pseudo-χ^2) to be given by the user. Optimal smoothing performance was achieved by setting this factor to 1.2 times the number of points to be fitted. All other spline fits mentioned in this report use the NAGLIB routine `E02BAE`.

[17] In the ARGUS software the *squared* resolution function values are kept in `TIDERF(128)`.

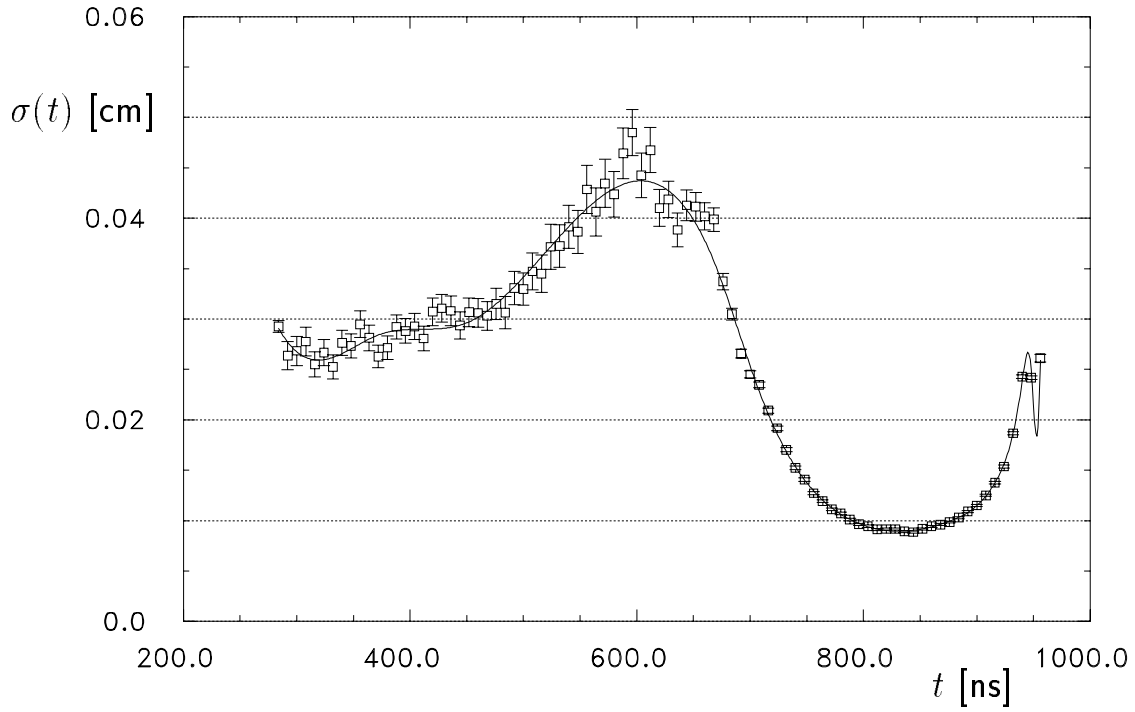

Figure 13: Resolution function $\sigma(t)$. Shown are the measured widths of the residual distributions (points with error bars) and the result of the spline fit (line).

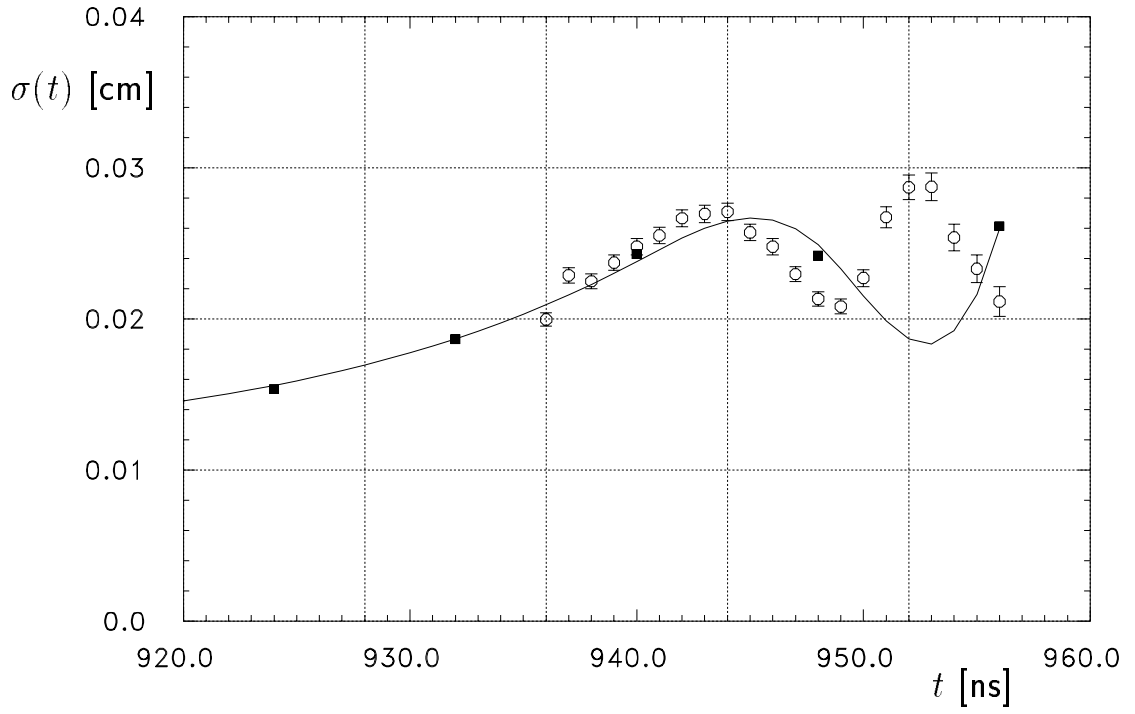

Figure 14: Resolution function $\sigma(t)$ close to the wire. Shown are the measured widths of the residual distributions in 8 ns bins (solid points) and in 1 ns bins (open points). The 8 ns bin limits are indicated by vertical dotted lines. The solid line is the result of the spline fit to the solid points.

- The resolution steadily rises up to $t = 944\,\text{ns}$. This is an effect of primary ionization statistics which causes non-Gaussian tails to develop on the negative sides of the $\Delta d(t)$ distributions (see Figure 9).

- As the drift distance sign selection procedure starts to fold the negative tails at $-d(t)$, the resolution goes down again in the time range $944 < t < 949\,\text{ns}$. This "improvement" clearly has nothing to do with drift chamber physics.

- As soon as the folded negative tails appear on the positive side of the $\Delta d(t)$ distributions, the resolution rises again in the time range $949 < t < 952\,\text{ns}$.

- All drift times beyond 952 ns correspond to $d = 0$. The variation in the measured times is mainly due to pulse rise time differences. Short rise times cause early wire signals which lead to large measured times. Hence the resolution apparently improves once more beyond 952 ns.

It must be kept in mind that the purpose of the resolution function $\sigma(t)$ is to provide the proper weight $1/\sigma^2(t)$ for each measured drift distance $d(t)$ which enters the least squares track fit. Especially in the cell region close to the wire $\sigma(t)$ then is different from the spatial resolution as defined by drift chamber physics processes, since the drift distance sign selection procedure enters its definition as well.

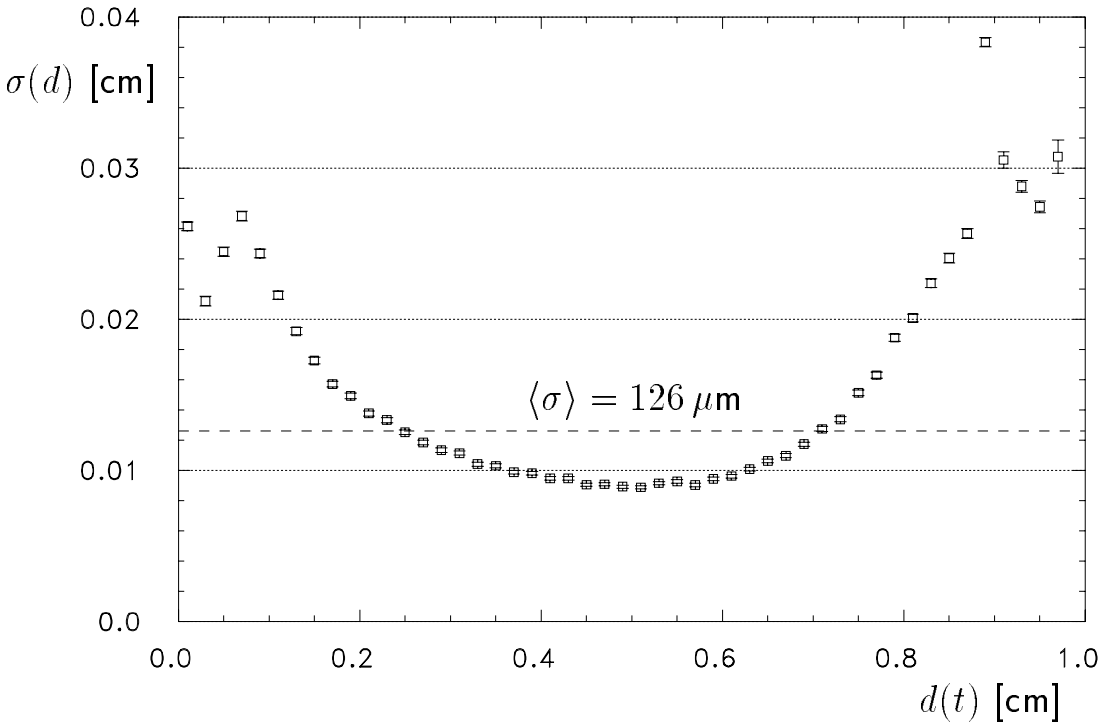

Figure 15: Resolution σ vs. drift distance d. The dashed horizontal line indicates the mean resolution according to (30).

Figure 15 shows the resolution σ as a function of the drift distance, determined from the distributions of scaled residuals in $200\,\mu$m bins of $d(t)$. Again the bad resolution around $d = 0.89\,\text{cm}$ clearly shows up.

A practical quantity for the global comparison of resolutions is the *mean resolution*

$$\langle\sigma\rangle = \frac{1}{\sqrt{\frac{1}{n}\sum_{j=1}^{n}\frac{1}{\sigma_j^2}}} \tag{30}$$

where σ_j is the resolution in the j-th of n equally sized drift distance bins. This definition of the mean resolution, via the average fit weight, takes into account that points with better resolution have a larger weight in the track fit. When used for track fitting, the mean resolution $\langle\sigma\rangle$ yields on average the same track parameter errors as the variable resolution from which it was calculated. Averaging the resolution $\sigma(d)$ shown in Figure 15 according to (30) yields a mean resolution $\langle\sigma\rangle = 126\,\mu$m.

7.8 Layer Time Shifts

Using the final DTR and resolution function for processing the calibration events, one finds that despite the application of the time corrections discussed in Section 6 there still remain slight systematic timing differences throughout the chamber. These are empirically parametrized by one individual time shift for each DC layer.[18] These time shifts are determined according to

$$\Delta t_{layer} = \frac{\langle\Delta d(t)\rangle_{layer}}{\langle v_{drift}\rangle}\ , \tag{31}$$

where only distance corrections from the time region of best spatial resolution ($770 < t < 900\,$ns) enter the layer average. The average drift velocity is calculated from the DTR:

$$\langle v_{drift}\rangle = \frac{d(770\,\text{ns}) - d(900\,\text{ns})}{130\,\text{ns}}\ . \tag{32}$$

8 Calibration Monitoring

8.1 Calibration Quality Measures

The quantities shown in Figure 16 demonstrate the quality of the calibration at this stage of the procedure. These results were obtained using the same DTR and resolution function for all drift cells.

- Figure 16a shows a perfectly flat distribution of the fitted distances of closest approach to the hit wires, i.e. the track fit reproduces the uniform irradiation of the drift cells. This is strong evidence that the DTR has been determined correctly.
- This is also demonstrated by Figure 16b which shows a zero average distance correction in the major part of the drift cell. The deviating behaviour around $d = 0$ results from the peculiar parametrization of the DTR in the region close to the sense wire. This essentially reflects the deviation of the crosses and the solid line in Figure 11.

[18] In the ARGUS software these are kept in `NTIDCA(36)`. Together with the crate time shifts `NTIDCR(9)` and the average trigger time `TIDBUN` they make up a set of CDT constants.

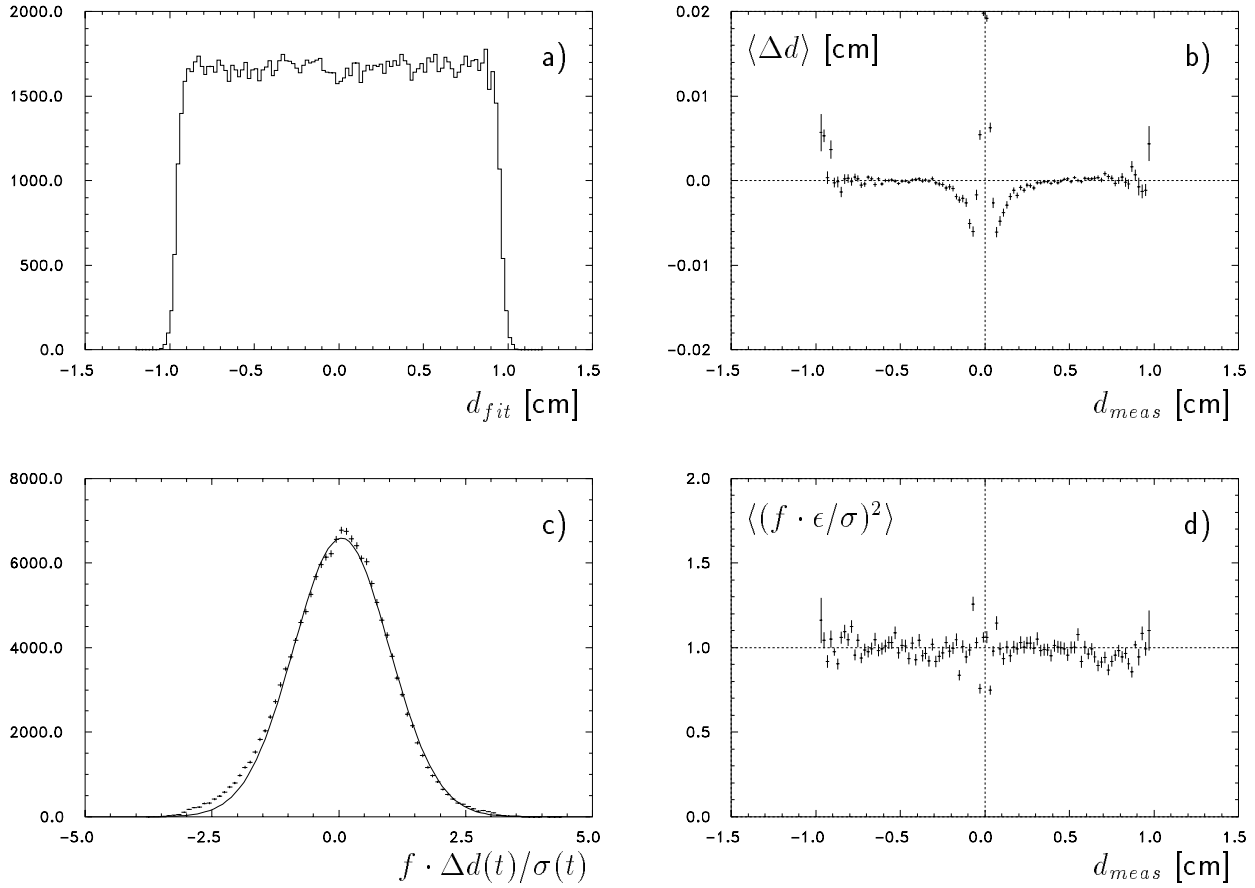

Figure 16: Some quantities demonstrating the calibration quality: (a) d_{fit} distribution; (b) mean distance correction $\langle \Delta d \rangle$ across the drift cell; (c) distribution of normalized scaled distance corrections $f \cdot \Delta d(t)/\sigma(t)$; (d) mean normalized variance across the drift cell.

- The distribution of normalized scaled distance corrections $f \cdot \Delta d(t)/\sigma(t)$ properly summarizes the information from all measured hits, despite the variable resolution across the drift cell. For normally distributed residuals one would expect this to be an $N(0,1)$-distribution, if the used DTR and resolution function are correct. The measured distribution shown by the crosses in Figure 16c has a mean value of 0.02 and an RMS error of 0.98, thus indicating a globally correct DTR and resolution function. The solid line is the result of fitting a Gaussian in the range $-1.0 \ldots 5.0$. The non-Gaussian tail on the negative side of the distribution clearly shows up by extension of the fit result to the full range. The origin of this tail was discussed in the context of Figure 9.

- A more detailed resolution check is presented in Figure 16d. The average normalized variance of the drift distance measurement $\langle (f \cdot \epsilon/\sigma)^2 \rangle$ has a flat distribution across the drift cell and a mean value around one. This shows that also locally the resolution function has been correctly determined.

- The flat fit probability distribution, almost identical to that shown in Figure 3a, is another indicator of properly determined calibration constants.

8.2 Calibration Constant Validity Ranges

Next one has to ensure that this calibration quality is maintained over the whole data taking period. In order to determine the validity ranges of the calibration constants, suitable quantities must be monitored as functions of real time. The ARGUS DC calibration monitoring procedure analyzes every tenth Barrel Bhabha event from the raw data tapes and plots the following quantities as functions of the run number:[19]

1. The mean event trigger time.
2. The mean number of hits per track $\langle n_{hit} \rangle$.
3. The mean normalized scaled distance correction $\langle f \cdot \Delta d(t)/\sigma(t) \rangle$ which must cluster around zero.
4. The mean fit probability $\langle \mathrm{prob}(\chi^2) \rangle$ which must cluster around 0.5.

The calibration constants need to be updated whenever a significant step shows up in any of these plots. Such changes can have a multitude of reasons, and it is difficult to formulate firm rules of what to do under which circumstances. A careful documentation of changes of the DC operating conditions (pressure, high voltage, amplifier threshold, exchanged electronics modules etc.) is definitely helpful. Using such additional information one can normally decide whether it is sufficient to adjust one or more of the various sets of time shift constants ($\rightarrow$ new *minor* calibration range), or whether a new DTR and resolution function are needed ($\rightarrow$ new *major* calibration range). Table 3 gives an overview of the major DC calibration ranges for the ARGUS runs with the μVDC installed. As an example, the calibration ranges for experiment

exp	runs	$\langle \sigma \rangle$ [μm]	$\langle n_{hit} \rangle$	# time shift adjustments	comment
9	75 – 203	138	34.3	8	initial calibration
	204 – 1075	126	35.3	14	V_{thr}: 1.8 $\rightarrow$ 1.4 mV
	1076 – 1117	123	35.4	1	p: 1042 $\rightarrow$ 1032 mbar
10	123 – 415	137	33.9	5	initial calibration
11	21 – 229	127	34.2	9	initial calibration
	230 – 278	130	34.4	4	no water vapour in DC gas
	279 – 349	129	34.2	5	water on again
	350 – 598	123	31.0	4	one defect TDC crate
	599 – 811	124	34.4	13	all crates up again
	812 – 1294	125	34.2	11	

Table 3: Major calibration constants validity ranges for the last three ARGUS data taking periods (experiments 9 – 11).

9 show how both $\langle \sigma \rangle$ and $\langle n_{hit} \rangle$ improve either by lowering the main amplifier threshold or by decreasing the chamber pressure, the latter being equivalent to increasing the high voltage.[20]

Having determined all required sets of DTR and resolution function and all sets of time shifts, the first round of the ARGUS DC calibration procedure is finished. All raw data tapes

[19] Typically one run corresponds to about one hour of data taking.

[20] The deterioration of the resolution due to the decreased primary ionization density is small compared to the improvement caused by the higher gas gain.

can now be processed, and based on the DC track reconstruction results a substantial data reduction takes place [1]. The accepted events are classified as Bhabhas, μ-pairs, multihadrons etc. which makes it easy to select events for the second phase of the DC calibration and for the calibration of other detector parts.

The procedure described so far is merely a revised version of the old DC calibration scheme. The major revisions include the more detailed handling of time corrections, the application of the residual scaling factor, the usage of calibration events with a flat $\cos\theta$ distribution, and the introduction of continuous calibration monitoring. The track fit inconsistencies discussed in Sections 3.2 and 3.3 were *not* cured by these modifications.

9 Pulse Shape Dependent Corrections

9.1 Origin of the Pulse Shape Dependent Timing

The ARGUS DC not only measures the trajectories of charged particles, but also their specific ionizations dE/dx, which are important ingredients for the charged particle identification procedure. The dE/dx of a particle is determined from the truncated mean of the signal charges recorded on the hit wires [1]. These are measured using charge sensitive ADCs (LeCroy System 2280). Only wires with an ADC/TDC coincidence are considered in the track fit and in the dE/dx analysis. This rejects much of the background from noise hits which inevitably occur if amplifier thresholds are kept low, aiming at the best possible spatial resolution.

In order to maintain the proportionality of primary ionization and measured pulse charge, the ARGUS DC must be operated at a relatively low gas amplification $A < 10^4$. This mode of operation maps all conceivable time structures of drift charge arrival at the sense wire into a large variety of different pulse shapes $V(t)$. These pulse shape variations significantly influence the drift time measurement, and the following study aims at finding suitable parameters for describing the effects.

9.2 Parametrization of the Pulse Shape Correction

The digital signal for the TDC start is generated as soon as the wire signal passes a preset amplifier threshold, i.e. the timing depends entirely on the leading pulse edge, not on the full pulse shape or even the pulse integral. The slope

$$\frac{dV}{dt} = \frac{1}{C}\frac{dQ}{dt} = \frac{I(t)}{C} \tag{33}$$

(C: drift cell capacity) of the leading edge determines the exact start time whereas its "granularity", introduced by the statistical nature of the current $I(t)$ and only partly smoothed by integrating time constants of the electronics, influences the time resolution. Hence it is sufficient to study the time dependence of the arrival of the *leading* drift charge at the sense wire. This is governed by several factors:

1. From pure drift cell geometry it follows that the number of leading primary ionization clusters arriving at the sense wire in a certain time interval Δt depends on the drift distance. Figure 17a shows two pairs of circular isochrones with the same spacing Δt at different drift distances. One can see how for a given ionization density the number of leading clusters in the time interval Δt decreases with decreasing isochrone radius, i.e.

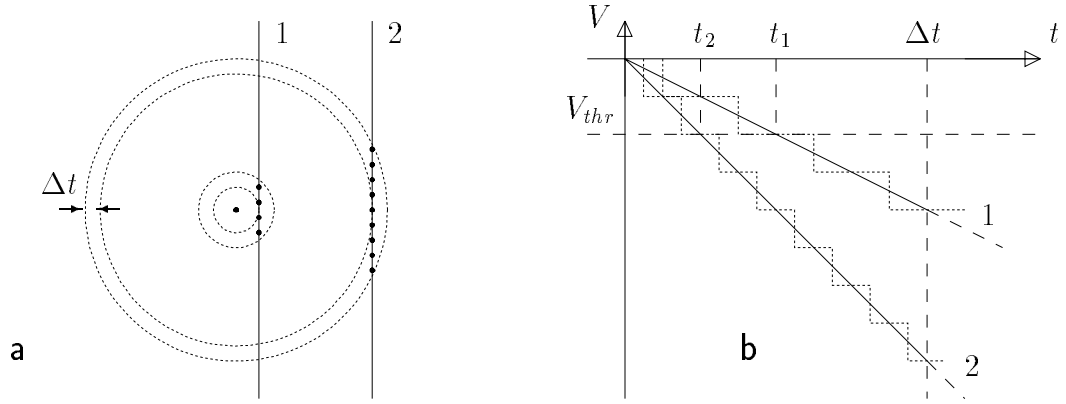

Figure 17: (a) Leading charge between isochrones with spacing Δt for two tracks at different drift distances (assuming $v_{drift} = const$) and (b) resulting voltage signals.

towards the sense wire. Figure 17b schematically shows the corresponding signal pulses. For simplicity it has been assumed that the arrival of each cluster leads to a drop of the signal voltage (dotted lines). The solid lines indicate the average leading pulse edges. At small drift distances (track 1) one obtains pulses with large rise times, the threshold V_{thr} is crossed later than for pulses from tracks through the central region of the drift cell (track 2). In addition to this time shift also the jitter of the threshold crossing time t_1 is larger than that of t_2, leading to a worse resolution at small distances.

This variation of the pulse shape with the drift distance and its influence on the drift time measurement is on average already contained in the calibration functions $d(t)$ and $\sigma(t)$, and no further corrections are required. For instance, Figure 15 clearly shows the deterioration of the resolution towards the sense wire.

Another distance dependent effect already contained in the DTR and the resolution function is the charge loss due to electron attachment which is caused by the 0.2 % water additive in the DC gas, and which increases with increasing drift distance.

2. For tracks through a given drift cell region the slope and jitter of the leading pulse edge still depend on the primary ionization density n_p which is proportional to the specific ionization dE/dx of the particle. Pulses from weakly and strongly ionizing particles show the same difference as the pulses 1 and 2 in Figure 17b.

   Since for the time measurement it does not matter at which point *along* a wire the drifting charges arrive, variations of the polar angle θ cause a similar effect as variations of the specific ionization, as illustrated by Figure 18. In the projection perpendicular to the sense wire one has an effective primary ionization density $n_p / \sin\theta$. Hence the combined dE/dx and θ dependence of the leading pulse edge is described by

$$\frac{dV}{dt} \propto \frac{dE/dx}{\sin\theta} \,. \tag{34}$$

3. The quantities discussed so far (d, dE/dx, θ) parametrize only the average rise time behaviour of pulses. On top of this, the statistical nature of the ionization process introduces random pulse shape fluctuations on a hit-by-hit basis. Such pulse shape differences from wire to wire are also caused by varying electronics gain factors or by variations of the

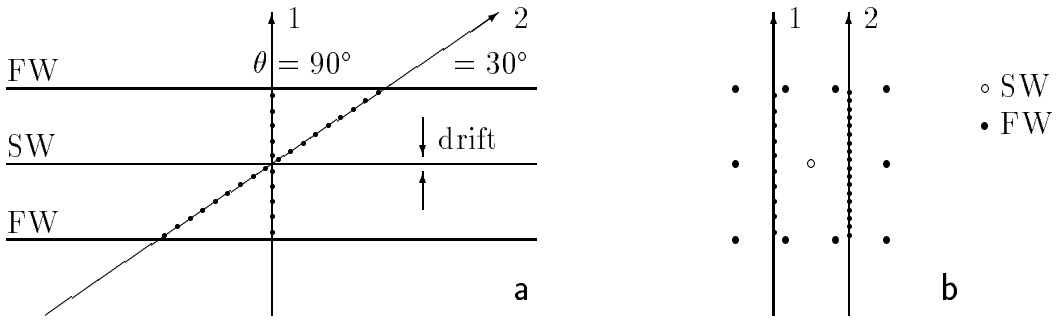

Figure 18: Sections through a drift cell (a) along the sense wire and (b) perpendicular to the wire with primary ionizations schematically indicated (SW/FW: sense/field wire). The projected ionization density in the plane perpendicular to the wire increases with decreasing polar angle of the track.

gas amplification, either due to different degrees of wire aging (increasing with decreasing layer radius) or due to the z-dependence of the sense wire position in the drift cell (see Section 2.1).

From the discussion of Figure 17 it follows that a pulse shape dependent timing correction must provide two things, namely a threshold crossing time shift $t_{thr} - t_{thr,0}$ and a resolution scaling factor σ/σ_0, where the reference values $t_{thr,0}$ and σ_0 are defined by the calibration event sample. Clearly the best way of taking pulse shape effects into account would be a rise time analysis on a hit-by-hit basis[21], but the charge sensitive ADCs used at ARGUS do not allow for this.[22] Instead the threshold crossing time shift and the resolution scaling factor are parametrized as functions of the track variables dE/dx and $\sin\theta$, i.e. all hits of a track experience the same correction. It is evident that this averaging method has its limitations, but it provides at least a global parametrization of the observed track fit anisotropy. For linearly rising pulses (34) yields the following dependence of the threshold crossing time on the selected parameters:

$$\frac{dV}{dt} \approx \frac{V_{thr}}{t_{thr}} \quad \rightsquigarrow \quad t_{thr} \propto \frac{\sin\theta}{dE/dx}\,. \tag{35}$$

The same behaviour follows for the resolution which is determined by the time jitter at the threshold level V_{thr}.

The extraction of the pulse shape dependent timing correction from data comprises two steps: First, a parametrization of the pure $\sin\theta$ dependence is determined for each major calibration range, using the corresponding calibration data sample. These Barrel Bhabhas have a uniform average energy loss $dE/dx = 6.5\,\mathrm{keV/2\,cm}$.[23] In a second step the dE/dx dependence, which is introduced as a universal scaling of the $\sin\theta$ argument of the polar angle correction, is checked using a sample of multihadron events, the only event class with tracks covering a wide range of dE/dx values.

[21] FADCs are the ideal electronic equipment for this purpose.

[22] The pulse integrals measured by these ADCs depend on too many other factors which have no influence on the pulse rise time, like the track length in the cell, the pulse cut-off due to the finite sampling gate length or the space charge effect at $\sin\theta = 1$. Assuming a linear relationship between pulse charge and rise time, i.e. a fixed pulse shape, an attempt was made to use the measured ADC values for a timing correction of individual hits, but this indeed failed.

[23] This actually is the reference value which the dE/dx calibration constants are adjusted to. The funny normalization to a length of 2 cm is adapted to the drift cell height in the ARGUS DC which varies between 1.6 and 2.0 cm (see Figure 1).

9.3 Polar Angle Correction

The $\sin\theta$ dependent threshold crossing time shifts are obtained in a similar way as described for the layer time shifts in Section 7.8. They are determined in bins of $\sin\theta$ from the observed distance corrections according to

$$\Delta t_{thr}(\sin\theta) = \left\langle \frac{\Delta d(t)}{v_{drift}} \right\rangle_{\sin\theta} \qquad \text{with} \qquad v_{drift} = \frac{d(t-1\,\text{ns}) - d(t+1\,\text{ns})}{2\,\text{ns}} \,. \tag{36}$$

The drift time is restricted to the range $720 < t < 900\,\text{ns}$ where the drift velocity is approximately constant and where the measured distance corrections are not biased by the systematic track fit effects discussed in Section 7.1. The resolution scaling factors are obtained from the widths of the distributions of the normalized scaled distance corrections (see Figure 16c for an example), accumulated in the same $\sin\theta$ bins. The data points in Figures 19a and b show examples of experimentally determined $\sin\theta$ corrections. The effect for Δt_{thr} is so strong that

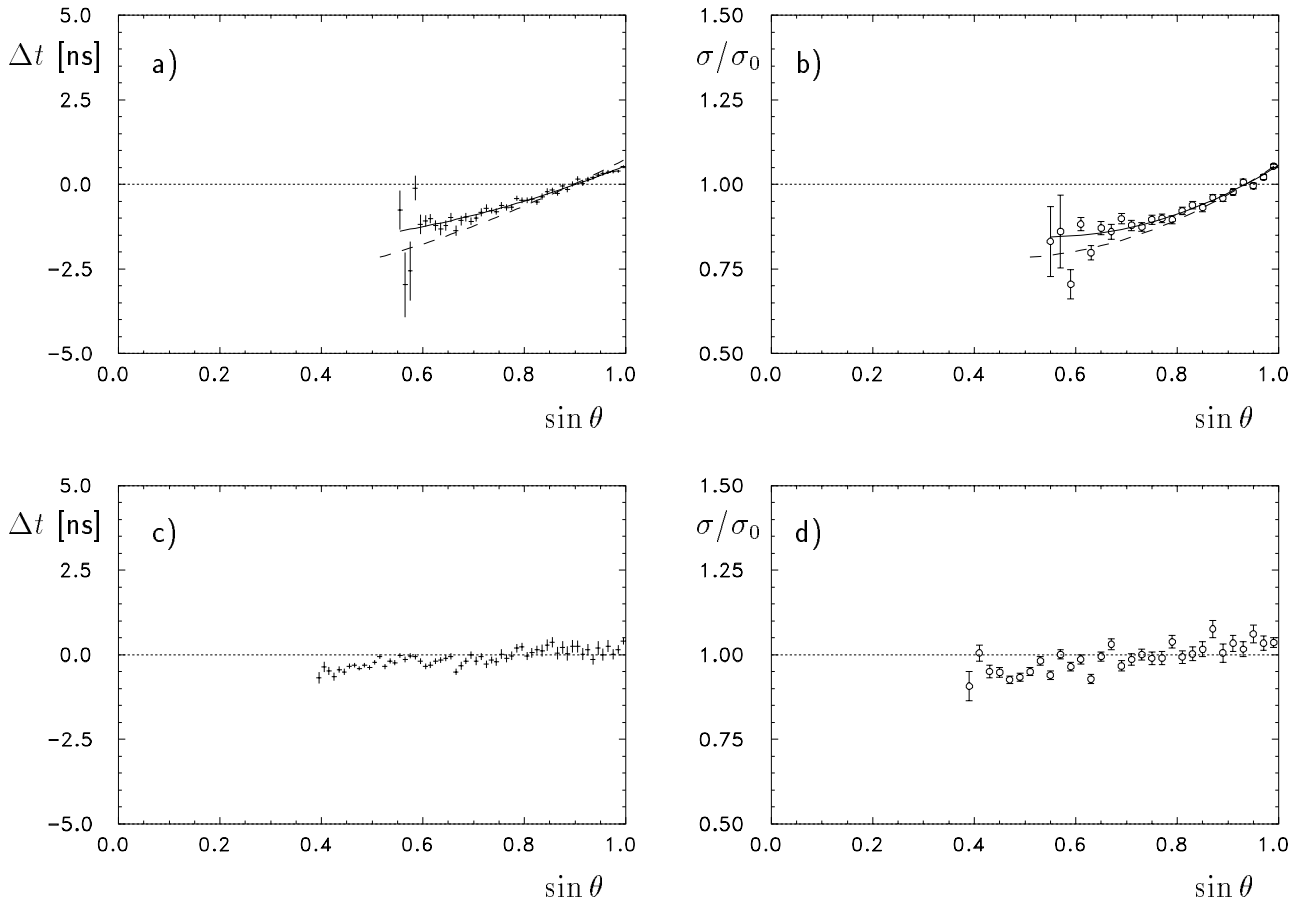

Figure 19: $\sin\theta$ dependent part of the pulse shape correction: (a) time shift and (b) resolution factor as determined from the calibration event sample (data points) together with fitted correction functions (solid lines); (c) time shift and (d) resolution factor as determined for full range Bhabha events with application of the fitted corrections from (a) and (b).

it results in a notable shift of the TDC spectrum (with all timing corrections of Section 6 applied) if events from different $\sin\theta$ intervals are analysed. Towards small $\sin\theta$ values, i.e. for large pulses, one observes a deviation from the linear behaviour predicted by (35), caused by

saturation. Allowing this effect to be different for the time shift and the resolution factor, both data are fitted with separate parabolic expressions

$$\Delta t_{thr}(\sin\theta) = a_1 + a_2(\sin\theta - a_3)^2 \quad (37)$$
$$\sigma/\sigma_0(\sin\theta) = b_1 + b_2(\sin\theta - b_3)^2 \quad (38)$$

The fit results are indicated by the solid lines in Figures 19a and b. For all hits of a track to be fitted, these parametrized corrections provide an additive time shift and a multiplicative resolution factor, both depending on the current estimate of $\sin\theta$. Using this polar angle correction in an analysis of *full range* Bhabha events ($\cos\theta < 0.92$),[24] produced the results shown in 19c and d. The corrections developed from Barrel Bhabhas ($\cos\theta < 0.80$) nicely extrapolate into the full polar angle region.[25] Using this correction, the polar angle dependence of the mean fit probability (see Figure 5) completely vanishes, the values are flatly distributed around 0.5. Hence the $\sin\theta$ dependent part of the pulse shape correction already solves the track fit anisotropy problem discussed in Section 3.3.

Within the time range mentioned above the polar angle correction proved to be largely independent of the drift time, thus demonstrating the validity of the simple leading pulse edge model over a wide range of drift distances.

The dashed lines in Figures 19a and b show the fitted correction functions for other data with a higher electronics threshold V_{thr}. As expected, the time slewing effect and the resolution deterioration are more pronounced.

9.4 dE/dx Correction

According to (35) the pulse shape dependent timing correction shows the same dependence on $\sin\theta$ and $\frac{1}{dE/dx}$. Assuming that the functional form is given by the $\sin\theta$ dependent parametrizations (37) and (38), the dE/dx dependence was introduced by the replacement

$$\sin\theta \to \left(\frac{\sin\theta}{dE/dx}\right)_{eff} \equiv \frac{\sin\theta}{1 + c\left(\frac{dE/dx}{6.5\,\mathrm{keV/2\,cm}} - 1\right)} \quad (39)$$

The parameter c serves to adjust the influence of dE/dx (or rather its deviation from the Barrel Bhabha average of $6.5\,\mathrm{keV/2\,cm}$) relative to that of $\sin\theta$. For $c = 1$ the variables $\sin\theta$ and $\frac{1}{dE/dx}$ have the same weight in the pulse shape correction. The value of c was adjusted by inspecting the flatness of the measured quantities Δt_{thr} and σ/σ_0 as functions of $\frac{1}{dE/dx}$ for a sample of multihadron events. Best results were obtained using the values 0.8 and 0.5 in the time shift and resolution factor parametrization, respectively (see Figures 20a to d). These values turned out to be universally applicable, i.e. valid for all calibration ranges listed in Table 3. Figures 20e and f demonstrate that the independence of the polar angle is maintained by the replacement (39).

There was also an attempt to determine the dE/dx dependence of the pulse shape correction using a procedure similar to the one described in Section 9.3 for the polar angle dependence.

[24] These were selected by requiring only 7 instead of 12 axial and stereo wires each, see also Section 7.3.

[25] It was also attempted to determine the polar angle correction using a full range Bhabha event sample. The hope was to improve the quality of the correction by basing it on the largest possible $\sin\theta$ range. However, it turned out that towards small $\sin\theta$ values especially the measured resolution factors are increasingly influenced by other effects than the pure polar angle dependence, the most severe of those being the quickly decreasing number of track hits.

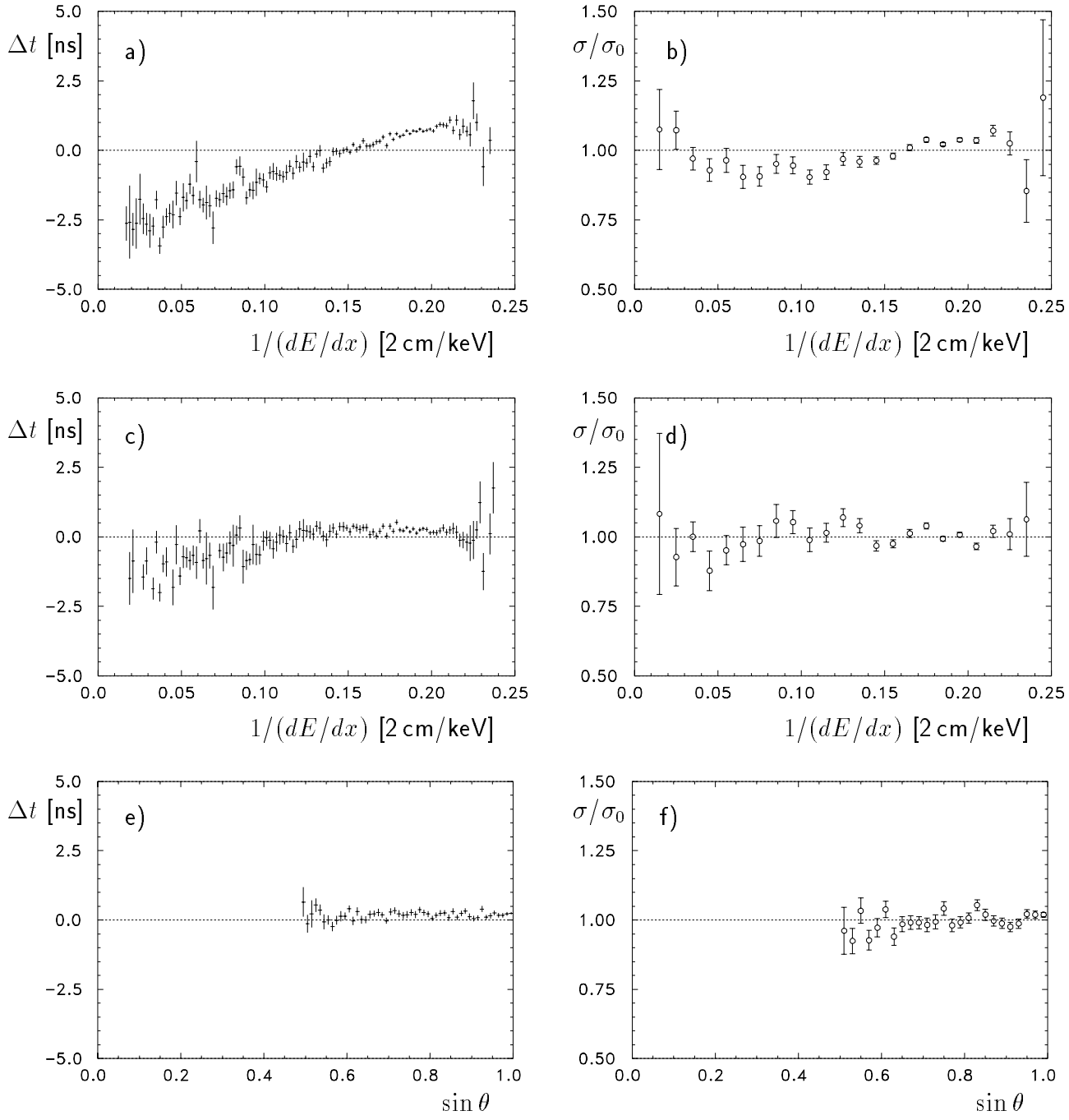

Figure 20: Effect of the pulse shape correction for multihadron events: (a) time shift and (b) resolution factor as functions of $\frac{1}{dE/dx}$ with polar angle correction only, (c) time shift and (d) resolution factor as functions of $\frac{1}{dE/dx}$ with the full pulse shape correction in effect, (e) time shift and (f) resolution factor as functions of $\sin\theta$ with the full pulse shape correction in effect.

This direct measurement of Δt_{thr} and σ/σ_0 in bins of $\frac{1}{dE/dx}$ had to be based on a sample of multihadron events in order to cover a reasonably large range of dE/dx values. However, most tracks in such events have small momenta — a median p_t of 370 MeV/c was observed for a typical multihadron event sample — resulting in a strong geometrical curvature and substantial

multiple scattering. These effects also cause deviations from the nominal calibration constants[26] and it becomes difficult to reliably isolate the dE/dx dependence. Hence this approach of determining the dE/dx correction was abandoned at some stage.

Inclusion of the pulse shape dependent timing correction notably improved the performance of the track reconstruction procedure for high momentum tracks ($p_t > 500\,\mathrm{MeV/c}$). The formerly observed polar angle dependence of the track fit probability vanished, and the reconstruction of Bhabha, μ-pair, multihadron and cosmic events yielded very similar results.

10 Isochrone Shape Correction

In the outermost region of the drift cell the isochrones are no longer circular as can be seen from Figure 2. While this is a general feature of drift chambers with cell limits defined by field wires instead of cylindrical metal tubes, the ARGUS DC offers additional complications: The sense wire is radially displaced from the cell center, this displacement varies along the wire, and it is different for axial and stereo wires (see Figure 1 and the discussion in Section 2.1). As a consequence the isochrones in the outer drift cell region in general exhibit no rotational symmetry whatsoever.

For a given drift time the DTR yields the drift distance corresponding to radial traversal of the drift cell since the calibration was done using almost straight Bhabha tracks. For different cell penetration angles there will be an angle-dependent correction to the drift distance obtained from the DTR. Due to the lack of any rotational symmetry the angular argument of this correction must be defined in the interval $[-\pi, \pi]$. A suitable quantity is the angle

$$\phi_{cell} = \phi_{track} - \phi_{wire} - \Delta\phi(z) = \arctan\frac{t_y}{t_x} - \phi_{wire} - \arctan\frac{z\tan\alpha}{r} \qquad (40)$$

This is the azimuthal angle of the point where a track touches the isochrone

PHICEL = PHIMOD(PHIT-PHIW-DPHI,0.0) IF (DRFDST.GT.0.0) PHICEL = PHIMOD(PHICEL+PI,(
C — GET CELL WIDTH RATZ = SQRT(TIDRA(ILAY)**2 + (DFZ(NST)*TANALF)**2)
WID = RATZ*TIDDP(ILAY) C — GET SENSE WIRE DISPLACEMENT FROM CELL
CENTER TANAUP = TIPST(1,ILAY)/SQRT(1.-TIPST(1,ILAY)**2) TANADN = TIPST(2,ILAY)/SQRT(1
TIPST(2,ILAY)**2) RUP = SQRT(TIPRA(1,ILAY)**2 + (DFZ(NST)*TANAUP)**2) RDN
= SQRT(TIPRA(2,ILAY)**2 + (DFZ(NST)*TANADN)**2) DISP = RATZ - (RUP+RDN)/2.

It is obvious that a correction to the nomi – show average res vs dmeas for Bhabhas first (axial – stereo)
– correction for isochrone shape (show muha plots, but important for all events: LR asymmetry for Bhabhas, mu-pairs)
– need 360 deg description, different for axial/stereo wires
– in bins of TDC
– p dependence (multiple scattering, show dp vs p plot)
– 6*phi is important Fourier component (cell geometry)
– 4*phi in more inward region
– why phi-dependent structure for small d?

[26] Strongly curved tracks in general do not traverse the drift cells radially. This effect is particularly disturbing in the outer region of the drift cell where the isochrones are no longer circular (see also Section 10). The plots shown in Figure 20 include only data from the inner drift cell region, corresponding to a drift time cut $t > 800$ ns, but still Figure 20c shows a slight under-correction for $dx/dx > 10\,\mathrm{keV}/2\,\mathrm{cm}$.

– if no dE/dx correction before, plot 41 doesn't go up to 0 (this lead initially to silly offset in constant term) i.e. important to have dE/dx first

11 Geometric Layer Alignment

– nasty plots: dp and dphi vs phi+
– are DC properties (exp 4=8, 9=10, 9.ne.8)
– possible deformation: non-concentric layers plus dphi
– determined by constraint fit to beam energy
– other possibilities ?
– mechanical fabrication ?

12 Calibration Prescription

The following list describes the calibration procedure for the ARGUS DC if starting from scratch. All programs and jobs can be found in the source library `F15KAP.DCCAL.S`.

1. Prepare a calibration dataset (job `#CALBHA` running program `*CALBHA`). This also yields the mean trigger time `TIDBUN`. Insert this into the initial CDT constants `@CDT0`.

2. Determine crate time shifts (job `#CRACAL` running program `*CRACAL`). All times are corrected using the individual trigger time. The member `@CDT0` is updated with the crate shifts.

3. Generate an integrated time spectrum (job `#INTEGR` running program `*INTEGR`). The initial set of CDS constants is stored in member `@CDS50`.

4. Analyze calibration events using the initial CDS constants (job `#CDSNEW` running the reconstruction program). Store new CDS constants in `@CDS51`. For the next iteration use these as input and so on. Switch to variable resolution (`LVARES = 1`) as soon as the DTR does not change anymore (usually after two iterations if starting from scratch). Stop if the mean resolution no longer changes (usually after three more iterations).

5. Determine the $\sin\theta$ correction using calibration Bhabhas (job `#CDSNEW` with `LTHECO = 1`). Use the same member for input and output CDS constants (only the $\sin\theta$ correction will be updated). Check the proper extrapolation of the correction to small $\sin\theta$ by analyzing *full range* Bhabhas in the run range of the calibration dataset (job `#CDSBHA`). A similar number of events is processed using the same CPU time if every 12-th Bhabha is analyzed. Add the dE/dx scale factor by hand and then insert the CDS constants member into your private constants file.

6. Run the calibration monitoring program `*CALMON` (job `#CALMON`) in order to determine the run ranges for which crate, CDT and CDS constants are valid. Whenever there occur jumps in the monitored quantities try to find out why (e.g. consult the run book, talk to the trigger expert). Then act accordingly:

   - Determine new crate shifts. If any of them has jumped, create a new set of CDT constants. Back to item 6 (once more monitoring).

- Create new CDT constants (job `#CDTNEW` running the reconstruction program). If they have changed, create a new set of CDT constants. Back to item 6 (once more monitoring).
- If all this does not help, a new major calibration range is needed. Back to item 4 (determine new CDS constants starting from the current set).

Only if all monitored quantities are behaving smoothly in the inspected run range proceed to the next item.

13 Some Results

– collection of final plots from RMS63TAP: E/B/M/C/H
– same table as in beginning
– compare with detector paper

14 Conclusions

– DC calibration procedure was improved, allows for consistent description of all relevant data
– leave discrepancies as they are, eventually fudge at later stage (vertex fit)

15 Acknowledgements

The DC track reconstruction software, the basis for any calibration attempt, was developed by H. Albrecht. The old calibration procedure was based on work by U. Binder and G. Harder [5]. During the development of the new procedure I benefitted much from discussions with H. Albrecht, A. Hüpper, S. Khan, B. Lewendel, E. Michel, S. Nowak, D. Reßing, K. Strahl, M. Walter and S. Weseler.

References

[1] H. Albrecht et al. (ARGUS Collaboration), Nucl. Instr. Meth. **A275** (1989) 1.

[2] E. Michel et al., Nucl. Instr. Meth. **A283** (1989) 544.

[3] V. Blobel, Least square methods, *in:* Formulae and methods in experimental data evaluation, vol. 3, ed. R. K. Bock et al., published by European Physical Society, 1983.

[4] H. Eichinger and M. Regler, Review of track fitting methods in counter experiments, CERN 81-06.

[5] G. Harder, Diplomarbeit, DESY Internal Report F15-84/01, November 1984.